MINERALOGICAL ASSOCIATION OF CANADA

Experiments at High Pressure and Applications to the Earth's Mantle

Short Course Handbook

Volume 21, May 1993
Edmonton, Alberta
Editor: R.W. Luth

Don R. Baker
Department of Earth and Planetary Sciences
McGill University
3450 rue Université
Montréal, QC, Canada H3A 2A7

Dante Canil
Bayerisches Geoinstitut
Universität Bayreuth
D-95440 Bayreuth, Germany

Thomas Chacko
Department of Geology
University of Alberta
Edmonton, AB, Canada T6G 2E3

Donald B. Dingwell, Nicholas S. Bagdassarov, Gilles Y. Bussod, Sharon L. Webb
Bayerisches Geoinstitut
Universität Bayreuth
D-95440 Bayreuth, Germany

Todd Dunn
Department of Geology
University of New Brunswick
Fredericton, NB, Canada E3B 5A3

Alan D. Edgar
Department of Geology
University of Western Ontario
London, ON, Canada N6A 5B7

Michael E. Fleet
Department of Geology
University of Western Ontario
London, ON, Canada N6A 5B7

Robert W. Luth
Department of Geology
University of Alberta
Edmonton, AB, Canada T6G 2E3

David C. Rubie
Bayerisches Geoinstitut
Universität Bayreuth
D-95440 Bayreuth, Germany

Reidar G. Trønnes
Geological Survey of Norway
P.O. Box 3006, Lade
N-7002 Trondheim, Norway

Michael T. Vaughan
Center in High-Pressure Research
State University of New York
Stony Brook, NY 11794-2100 USA

TABLE OF CONTENTS

Chapter 1

Apparatus and Techniques for Experiments at Mantle Pressures

Robert W. Luth

Chapter 2

Measurement and Control of Intensive Parameters in Experiments at High Pressure in Solid-media Apparatus

Robert W. Luth

Chapter 3

The Piston-Cylinder Apparatus

Todd Dunn

Chapter 4

In-Situ X-ray Diffraction Using Synchrotron Radiation at High *P* and *T* in a Multi-Anvil Device

Michael T. Vaughan

Chapter 5

Magma Rheology

D. B. Dingwell, N. S. Bagdassarov, G. Y. Bussod, and S. L. Webb

Chapter 6

Phase Equilibria at High Pressures Applied to the Earth's Mantle

Dante Canil

Chapter 7

Mechanisms and Kinetics of Reconstructive Phase Transformations in the Earth's Mantle

David C. Rubie

Chapter 8

Measurement of Diffusion at High Temperatures and Pressures in Silicate Systems

Don R. Baker

Chapter 9

Experimental Studies of Equilibrium Oxygen and Carbon Isotopic Fractionation Factors Between Phases

Thomas Chacko

Chapter 10

Small Degrees of Partial Melting in the Mantle and Mantle Metasomatism: An Experimental View

Alan D. Edgar

Chapter 11

Fe-Ni-S-O System: Phase Relations, Partitioning of Siderophile Elements, and Applications to the Earth

Michael E. Fleet

Chapter 12

Volatile-bearing Phases in the Earth's Mantle

Robert W. Luth, Reidar G. Trønnes, and Dante Canil

MAGMA RHEOLOGY

D.B. Dingwell, N.S. Bagdassarov, G.Y. Bussod and S.L. Webb

Bayerisches Geoinstitut
Universität Bayreuth
D-95440 Bayreuth
Germany

5.1. INTRODUCTION

Igneous processes are currently viewed as the chief agent of mass and heat transport contributing to the development of the chemical, physical and mineralogical differentiation of the Earth's crust and upper mantle. Accordingly, the mechanism for all of this differentiation, the movement of silicate melts during each stage of igneous petrogenesis, is one of the central themes in experiments, calculations and the interpretation of field observations both on exposed, extinct plutonic systems and on volcanic systems, active or dormant. The scope of the discussion is immense and the methods used are numerous. The basic nature of the materials changes from liquids, through foams, emulsions, crystal suspensions, and partially molten aggregates. The rheology of such widely varying materials, each complex in its own right, defies a simple description. Up to this stage in the research on geologically relevant materials, however, most of the possible options for deformation and transport behavior of magmas have been presented in the literature and much experimental work has been accomplished. We review in this contribution the rheology of melt-bearing systems. We hope to illustrate clearly the fundamental aspects of silicate melts which link the various melt-based systems together as well as the critical differences in rheology which distinguish them.

We begin with a look at the rheology of silicate melts, covering the state of knowledge of the measurement of viscosity, its dependence on composition, temperature, pressure and strain-rate, and predictive calculation schemes. We turn next to two-phase suspensions where the distribution and redistribution of the included crystals is a significant complication. Bubble-bearing systems are reviewed next where the deformation of the included phase becomes yet another significant factor in determining the rheology. Finally, we go beyond the rheologically critical melt percentage (RCMP) to treat the flow of partially melted aggregates where solid-solid interactions can dominate flow. Volcanic rocks have performed the entire journey, from the rheological point of view truly a remarkable one, to the surface of the Earth.

5.1.1. Definitions

A Newtonian fluid is one for which a linear relation exists between stress and the spatial variation of velocity. The *viscosity* of a Newtonian material is defined as the ratio of stress to strain-rate

$$\eta = \frac{\sigma}{\dot{\varepsilon}} . \tag{5.1}$$

The *elastic modulus* of a Hookean elastic material is defined as the ratio of stress to strain

$$M = \frac{\sigma}{\varepsilon} . \tag{5.2}$$

As is the case for elastic moduli, we can, for an isotropic medium like a silicate melt, speak of two components of viscosity, a volume and a shear component. The combination of volume and shear viscosity yields a longitudinal viscosity

$$\eta_l = \eta_v + \frac{4}{3}\eta_s . \tag{5.3}$$

A comparison of longitudinal and shear viscosities illustrates that volume and shear viscosities are sub-equal at very low strains (Dingwell and Webb, 1989) (see Fig. 5.1). The ratio of Newtonian viscosity to elastic modulus yields a quantity with dimensions of time. This ratio

$$\tau = \frac{\eta}{M} \tag{5.4}$$

is the Maxwell *relaxation time* (Maxwell, 1867). This relaxation time is a convenient approximation to the timescale of deformation where the transition from purely viscous behavior to purely elastic behavior occurs. According to this convention, the purely viscous response of a silicate melt is termed "liquid" behavior whereas the purely elastic response is termed "glassy" behavior. The term silicate *melt* is used to describe molten silicates quite generally, regardless of their rheology. Even for the simple case of a Maxwell body, the change from "liquid" to "glassy" behavior does not occur as a sharp transition but rather describes a region of mixed liquid-like and solid-like behavior, a region of

viscoelastic response. Deformation experiments performed in the viscoelastic region contain three distinct time-resolved components of deformation, instantaneous recoverable, delayed recoverable and delayed non-recoverable. Figure 5.2 illustrates these components for a creep experiment. Viscous flow is the delayed non-recoverable component, the term anelasticity refers to the instantaneous plus the delayed recoverable deformation and the entire deformation behavior falls under the heading of *viscoelasticity* (Nowick and Berry, 1972).

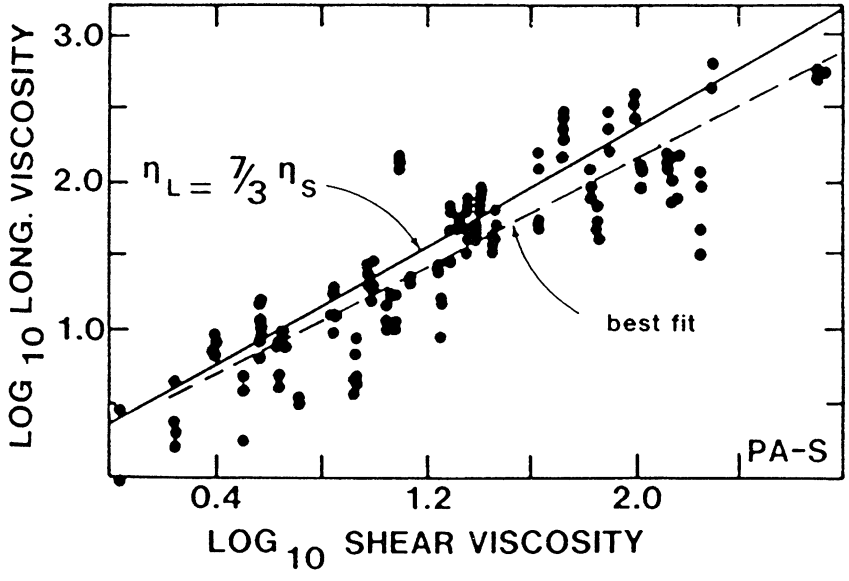

Figure 5.1. The relationship between longitudinal and shear viscosities in silicate melts. The solid line represents the correlation predicted from the assumption that volume and shear viscosities are equal. The dashed line is the best fit to the data and lies within one standard deviation of the theoretical line. The longitudinal viscosities are from Rivers & Carmichael (1987). The shear viscosities are from various studies in the literature. (Redrawn from Dingwell and Webb, 1989.)

Geological materials can possess a more complicated rheology than a simple viscoelastic liquid with one relaxation time. The combination of a number of Maxwell elements is required to adequately describe the strain-rate dependent rheological behavior of geomaterials. Thus the main goal of laboratory experiments is to observe the rheological properties of geomaterials at the strain-rate and P-T conditions appropriate for geological processes. Inasmuch as

temperature and pressure affect viscosity, the Maxwell relaxation time [Eqn. (5.4)] varies with ambient conditions, and thus the dimensionless variable $\dot{\varepsilon}\tau$ is an appropriate parameter for the comparison of materials with different rheologies, obtained at different timescales and P-T conditions.

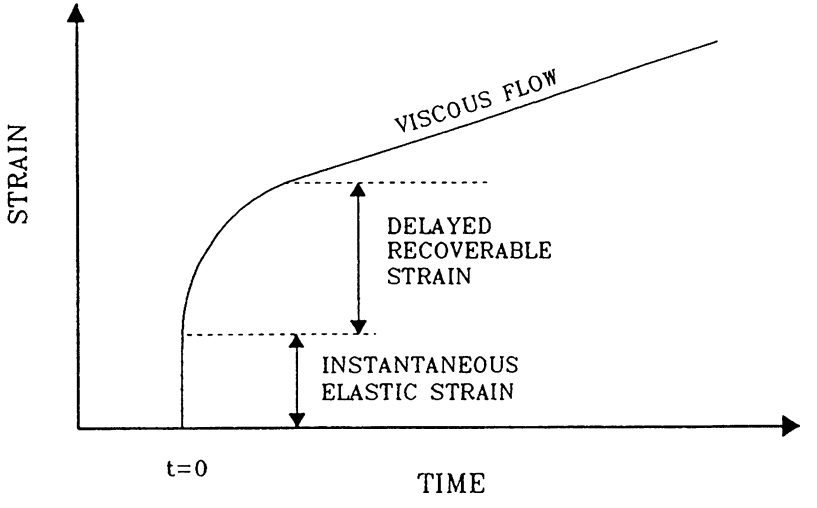

Figure 5.2. The instantaneous recoverable elastic strain, the delayed recoverable strain and the delayed non-recoverable strain (viscous flow) occurring in a linear viscoelastic material upon application of a step function in stress at time t=0.

Structural relaxation in silicate melts is but one example, the simplest, of a relaxation mode. It can be mechanically represented as a series combination of viscous dash-pot and elastic spring (a Maxwell element). In more complex materials such as crystal suspensions, foams and partial melts, several additional mechanisms of deformation are contributed at distinct timescales of deformation via additional relaxation modes within and between the added phases (*e.g.* crystal-crystal interactions, bubble deformation, matrix compaction). These relaxation modes involve chemical and textural equilibria and thus occur at increasingly longer timescales, *i.e.* at lower rates of deformation. As a consequence of the multiphase nature of flowing magma, the accompanying mechanical models become more complex involving additional viscoelastic elements in the linear regime and non-linear effects as well. Inherent in the experimental study of magma rheology then is the experimental deformation rate or its inverse the

experimental timescale. It is this experimental deformation rate which must most closely match natural processes in order to make secure applications of rheological measurements.

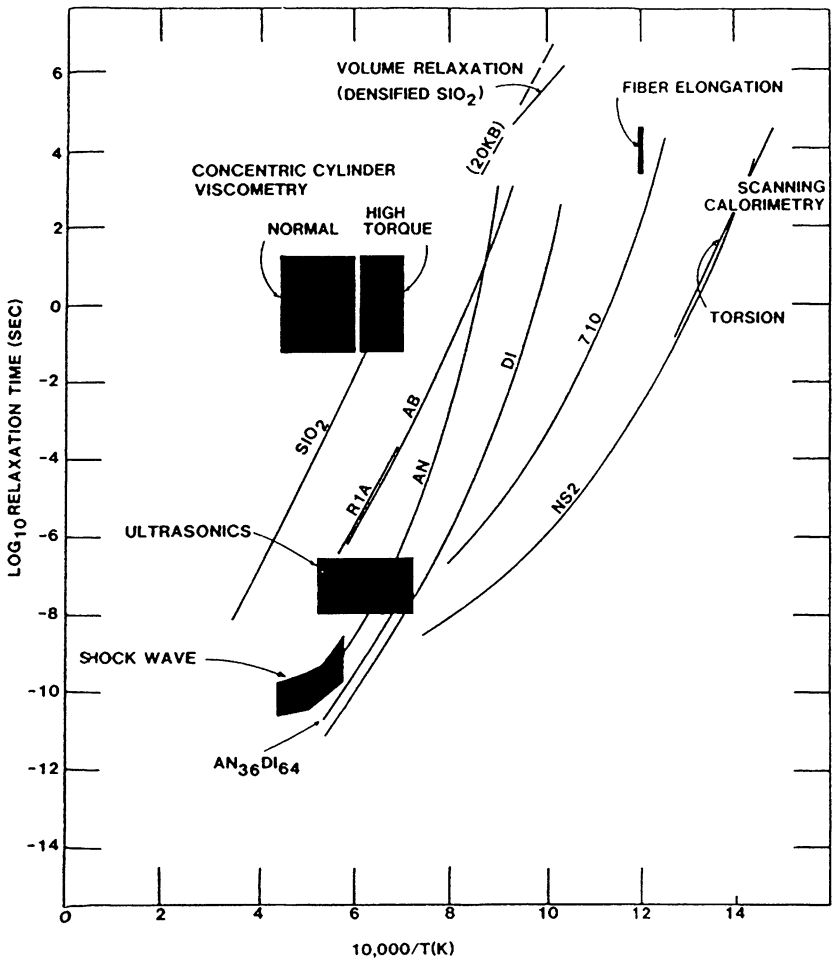

Figure 5.3. The liquid-glass transition as a function of temperature for several silicate melts calculated from Eqn. (5.4) together with the timescales on which a range of experimental measurements are performed. The relaxation times relating to the various experimental techniques are discussed in Dingwell and Webb (1989). (Redravn from Dingwell and Webb, 1989.)

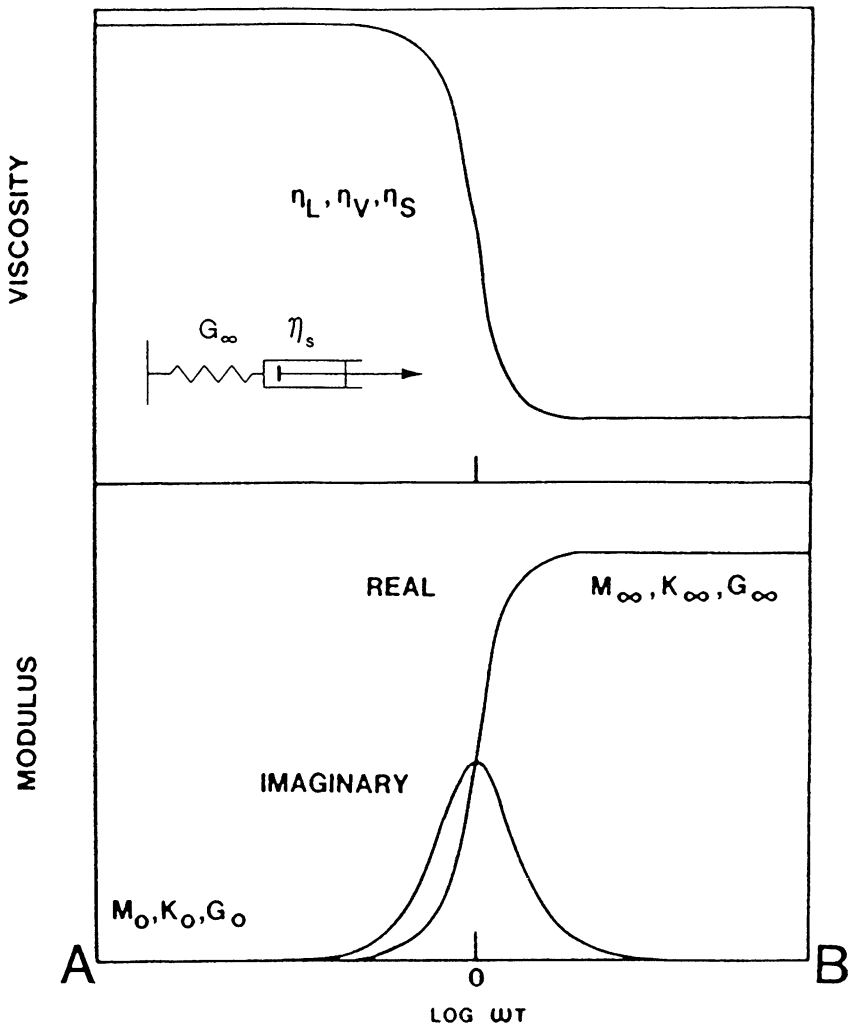

Figure 5.4. Calculated frequency dependent behavior of longitudinal, volume and shear viscosities (η_l, η_v, η_s) and moduli (M, K, S) of a linear viscoelastic melt with a relaxation time τ, plotted as a function of $\omega\tau$, where ω is the angular frequency of the applied sinusoidal stress. The subscripts "0" and "∞" indicate zero frequency and infinite frequency values. The shear relaxation time $\tau_s=\eta_s/G_\infty$ is for the simple mechanical Maxwell model of a spring and dash-pot in series.

5.2. CLASSES OF EXPERIMENTS

In principle, any experiment that records strain as a function of time and applied stress can be used to obtain viscosity. Viscosity experiments can be subdivided in several ways. We can for example, distinguish between those in which the strain-rate is controlled and the resultant stress is measured (*e.g.* concentric cylinder) and those in which the stress is controlled and the resultant strain-rate is measured (*e.g.* fiber elongation). We can also separate those methods which involve only shear stresses (*e.g.* concentric cylinder) from those which involve a combination of shear and compressive or dilatational stress (*e.g.* beam bending or fiber elongation). For any given geometry which employs controlled strain we can further distinguish between the application of a step function of strain and the continuous application of strain (*e.g.* stress relaxation versus steady-state flow). Stress relaxation involves the recording of stress versus time as the stress field decays to zero after the application of a step function of strain. Steady-state strain experiments record the equilibrium stress sustained by the melt due to the constant strain-rate being applied to the melt. We can distinguish between experiments performed at low total strains such that the perturbations from equilibrium are small and in the linear regime of stress-strain relations. Such measurements probe the response of the system to stresses without macroscopic rearrangement of the structure. In contrast, nonlinear measurements can deal with the redistribution of phases during macroscopic flow. Finally, we can distinguish between time domain experiments where a stress is applied and the time variant relaxation of the system to the new equilibrium is measured (*e.g.* creep experiments) and frequency domain experiments where sinusoidal variations of the stress field, small in magnitude but up to very high frequencies (from mHz to MHz) are applied and the magnitude and phase shift of strain is measured (*e.g.* ultrasonic wave attenuation). Implicit in considerations of rheological measurements is the ratio of the deformation rate to the relaxation rate of structural components in the material. The characteristic strain-rate of the experiment is easily defined in most rheological experiments. For example, in Fig. 5.3 several experimental timescales are compared with structural relaxation times of silicate melts. Ultrasonic measurements are performed on timescales of 1-50 ns, forced oscillation techniques in the range of 0.01-150 s and fiber elongation from 10^2 to 10^6 s. Each component or phase of the system may contribute one or more distinct relaxation modes at distinct timescales which are functions of pressure and temperature. Frequency-dependent or non-Newtonian effects are seen in frequency domain rheological experiments when the measurement timescale approaches a relaxation mode timescale (see Fig. 5.4).

5.2.1 Geometries

a. Couette

The most widely used example of controlled strain-rate and measured stress is the rotational (Couette) method (see Fig. 5.5). Ryan and Blevins (1987) provide a description of the physics of Couette viscometry. The strain-rate is imposed on an annulus of liquid filling the gap between an inner cylinder (or spindle) and the outer cylinder (or cup) which usually takes the form of a cylindrical crucible. The strain-rate is delivered to the liquid by rotating either the inner or outer cylinder. The shear stress sustained in the liquid is usually recorded as the torque exerted by the liquid on the inner cylinder. In rotating spindle viscometers the spindle is often driven at set speeds by a step motor. The spindle is set on a low friction jewel bearing and is connected to a rotational displacement transducer which produces a mV signal proportional to torque. The concentric cylinder method is usually employed as a relative measurement technique. Viscosity standards are used to calibrate the instrument at varying conditions of temperature and strain-rate. These calibration curves are then used to convert the sample torque data into viscosity values. The concentric cylinder method is commonly used for viscosity measurements in the range of 10^{-1}-10^{5} Pa s.

Another form of the Couette viscometer is the cone-and-plate geometry. Viscometers based on the cone-and-plate geometry have been used in both steady state (as above) and pulse strain modes. The geometry of the cone-and-plate viscometer allows the preparation of starting materials by pre-machining to the final form. This avoids the need to pour or melt the silicate material into the cylinder and to immerse the spindle into the liquid at high temperature. The cone-and-plate method finds application at lower temperatures and higher viscosities than the concentric cylinder method. This method has also been used in the investigation of the viscoelastic behavior of silicate melts at near the glass transition (Simmons *et al.*, 1988).

b. Fiber Elongation

Shear viscosities in the range 10^{9}-10^{14} Pa s can be determined using fiber elongation techniques (see Fig. 5.5). Melt fibers with a diameter 0.1-0.3 mm and lengths 10-18 mm are commonly used. The ends of the fibers are formed into beads using an oxy-acetylene flame. In a vertical mounted silica glass dilatometer, the silica glass holder of the dilatometer supports the beaded melt fiber in a fork. A second silica glass rod holds the lower bead of the fiber in tension. The strain-rate range is machine limited to 10^{-7}-10^{-4} s^{-1}. A tensile stress (~10^{7} Pa) is applied to the melt fiber and the viscosity is determined as the ratio

of the applied stress to the observed strain-rate. In this geometry, the observed viscosity η_{elong} is the elongational viscosity and is related to the shear viscosity η_s by

$$\eta_{elong} = \frac{\sigma}{\dot{\varepsilon}} = \frac{9\,\eta_v\,\eta_s}{3\eta_v + \eta_s} \tag{5.5}$$

where η_v is the volume viscosity (*e.g.* Herzfeld and Litovitz, 1959; Ferry, 1980; Mazurin, 1986) for stress σ, and strain-rate $\dot{\varepsilon}$. The accuracy of the viscosity measurements ranges from ± 0.1 to ± 0.01 $\log_{10}$ Pa s, with increasing strain-rate. Although infinite shear strains are possible in a melt, volume strain must be limited in magnitude (Mazurin, 1986). The volume viscosity of a melt therefore approaches an infinite value with increasing time and Eqn. 5.5 becomes

$$\eta_{elong} = 3\,\eta_s \tag{5.6}$$

(Ferry, 1980; Mazurin, 1986) for times greater than the relaxation time of the melt. Equation 5.6 is known as Trouton's rule.

The elongation of liquid fibers yields viscosity data for stresses which do not exceed the tensile strength of silicate melts. Liquid fibers must be drawn from high temperature melts at the correct conditions of drawing speed and viscosity to obtain fibers of circular cross section and the required diameter.

c. Micropenetration

Absolute shear viscosities in the range 10^9-10^{11} Pa s can be determined using micropenetration techniques (see Fig. 5.5). This involves determining the rate at which an indenter under a fixed load moves into the melt surface. High accuracy (± 0.1 $\log_{10}$ Pa s) is obtained by using a silica glass sample holder and pushrod for temperatures under 1000°C. The indenter may be conical, cylindrical or spherical in shape (Brückner and Demharter, 1975). For the case in which a spherical indenter is used (*e.g.* Dingwell *et al.* 1992) the absolute shear viscosity is determined from

$$\eta_s\,(\text{Pa s}) = \frac{0.1875\,P\,t}{r^{0.5}\,l^{1.5}} \tag{5.7}$$

(Pocklington, 1940; Tobolsky and Taylor, 1963) for the radius of the sphere r (m), the applied force P (N), indent distance l (m), and time t (s) (t=0 and l=0 upon application of the force). The system of Dingwell *et al.* (1992) uses 3 mm

diameter precision spheres of alumina and a force of 1 N. The melt samples are cylinders of 8 mm diameter which are at least 3 mm thick. The measurements are performed over indentation distances less than 300 μm as Eqn. 5.7 is derived on the assumption that the indentation distance is much less than the radius of the indent sphere (l<<r). With 3 mm thick samples, together with an indentation distance less than 300 μm and an indenter radius of 3 mm, no edge effects and no end effects are observed over the range 10^9-10^{11} Pa s. Previous studies of the shear viscosity of silicate melts in the range 10^6-10^{12} Pa s (*e.g.* Hummel and Arndt, 1985; Tauber and Arndt, 1986; Tauber and Arndt, 1987) have used hemispherical metal indenters with a diameter of 0.6 mm and a slightly different formula to calculate the shear viscosity.

d. Parallel Plate

The shear viscosity of large cylinders of melt or partially molten material can be determined by deforming the cylinder between parallel plates moving perpendicular to their faces. Absolute viscosities in the range 10^4-10^8 Pa s (Gent, 1960; Fontana, 1970) and 10^7-10^{11} Pa s (Bagdassarov and Dingwell, 1992) can be determined. Specimen deformation rates are measured with a linear voltage displacement transducer. For a cylindrical specimen of any thickness, the shear viscosity can be determined by

$$\eta_s \text{ (Pa s)} = \frac{2\pi m g h^5}{3V \delta h/\delta t (2\pi h^3 + V)} \qquad (5.8)$$

for the applied mass m (kg), the acceleration due to gravity g, the volume V (m^3) of the material, the height h (m) of the cylinder and time t (s) (Gent, 1960; Fontana, 1970), for the case in which the surface area of contact between the melt and the parallel plates remains constant and the cylinder bulges with increasing deformation. This is the "no-slip condition". For the case in which the surface area between the cylinder and the plate increases with deformation and the cylinder does not bulge, the viscosity is

$$\eta_s \text{ (Pa s)} = \frac{m g h^2}{3V \delta h/\delta t}. \qquad (5.9)$$

This is the perfect slip condition.The parallel plate method involves the uniaxial deformation of a cylinder of melt, at either constant strain-rate (*e.g.* Hessenkemper and Brückner, 1989) or constant load (*e.g.* Shiraishi *et al.*, 1987). Constant strain-rate experiments yield stress-time relationships that can be

sensed with a load cell. Constant load experiments yield strain-time relationships determined by dilatometry. Care must be taken to ensure parallel faces of the sample. Uneven faces result in anomalously high strain-rates due to reduced initial cotact area.

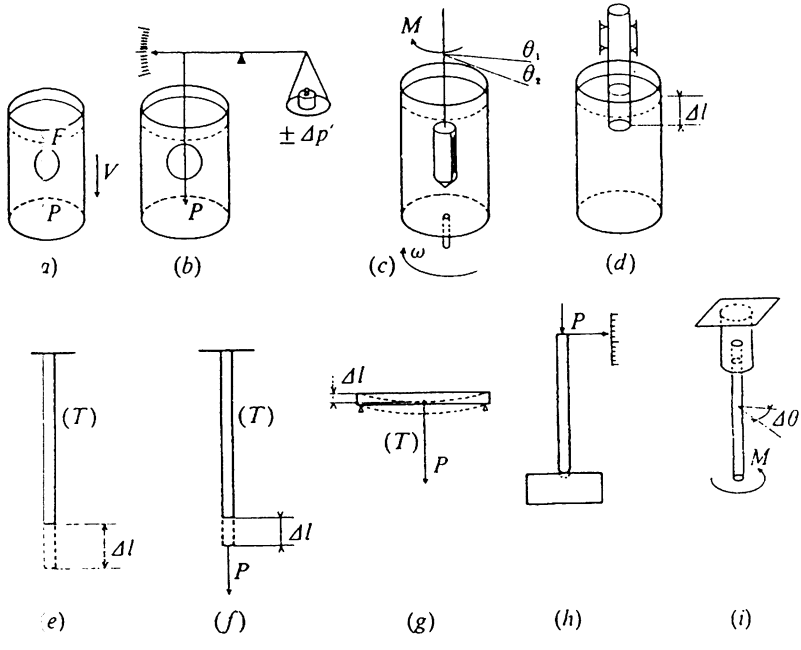

Figure 5.. Methods of determining viscosity: (a) falling sphere, (b) counterbalanced sphere, (c) Couette viscometer, (d) sink point measurement, (e) free fiber elongation, (f) loaded fiber elongation, (g) beam bending, (h) micropenetration, (i) torion of a cylinder. (Redrawn from Zarzycki, 1991.)

e. Falling Sphere

The counterbalanced sphere and falling sphere viscometers (see Fig. 5.5) are based on Stokes law. Riebling (1963) has described a counterbalanced sphere viscometer which he subsequently used in viscosity determinations in the B_2O_3-SiO_2 (Ribling, 1964) and Na_2O-Al_2O_3-SiO_2 (Riebling, 1966) systems. Falling sphere viscometry has been employed at 1 atm and at high pressures (*e.g.* Shaw, 1963; Fujii and Kushiro, 1977; Ryan and Blevins, 1987). The falling sphere method may be used for the simultaneous determination of density and viscosity. Alternatively, the falling sphere method may be used with input values of density provided the density contrast between melt and sphere is relatively large.

Maximizing the density contrast reduces errors associated with the estimation of melt density. Errors in density contrast can easily be reduced below the uncertainties inherent in the other variables affecting viscosity determination. Shaw (1963) used the falling sphere method in hydrothermal pressure vessels to determine the effect of water on rhyolite viscosity to 0.2 GPa. The method was applied to higher pressures in the piston cylinder apparatus by Fujii and Kushiro (1977) and since that study the method has been widely used (*e.g.* Scarfe *et al.*, 1986; Dingwell, 1987; Brearley and Montana, 1989; and White and Montana, 1990). Fujii and Kushiro (1977) tapered the graphite furnace to obtain a reduced temperature gradient of 8°C cm^{-1} at pressures to 2.25 GPa. The temperature gradient alone generates an error of 10% in viscosity. Total errors for falling sphere viscosity determinations using the piston cylinder apparatus are probably nearer 20%. Most high pressure studies using the falling sphere method have relied on quenching the sample, sectioning the charge and measuring the sphere displacement by optical or radiographic methods (Hazen and Sharpe, 1983). Burnham (1963) describes a variant on the falling sphere method in which the fall of a sphere, connected to a wire isolated electrically from the metal capsule, was electrically detected by the contact of the sphere against the capsule wall. Persikov *et al.* (1990) used a radioactive-tracer doped falling sphere in an internally-heated pressure vessel. The descent of the sphere is recorded radiographically as the sphere transits two "windows" in a lead shield. Very high pressure measurements of viscosity have been made by Kanzaki *et al.* (1987) who imaged the falling sphere in real time using a synchrotron radiation source and a MAX 80 super-press. This method extends the lower limit of measurable viscosity using the falling sphere method at high pressure to 10^{-3} Pa s (see Fig. 5.6).

f. Capillary Extrusion Viscometer

A capillary extrusion viscometer for use with silicate melts has been described by Mills and Pincus (1970) who refer to its wide use in polymer studies. The apparatus consists of a "syringe" machined from graphite. Mills and Pincus (1970) set the strain-rate and monitored the resultant stress with a load cell. The viscometer was used with melt viscosities from 10^{-1} to 10^{5} Pa s and strain-rates up to 10^{3} s^{-1}. An extensive discussion of the relevant equations and corrections is provided by Mills and Pincus (1970). A similar device was used by Dane and Birch (1938) to measure the pressure-dependence of B_2O_3 melt viscosity.

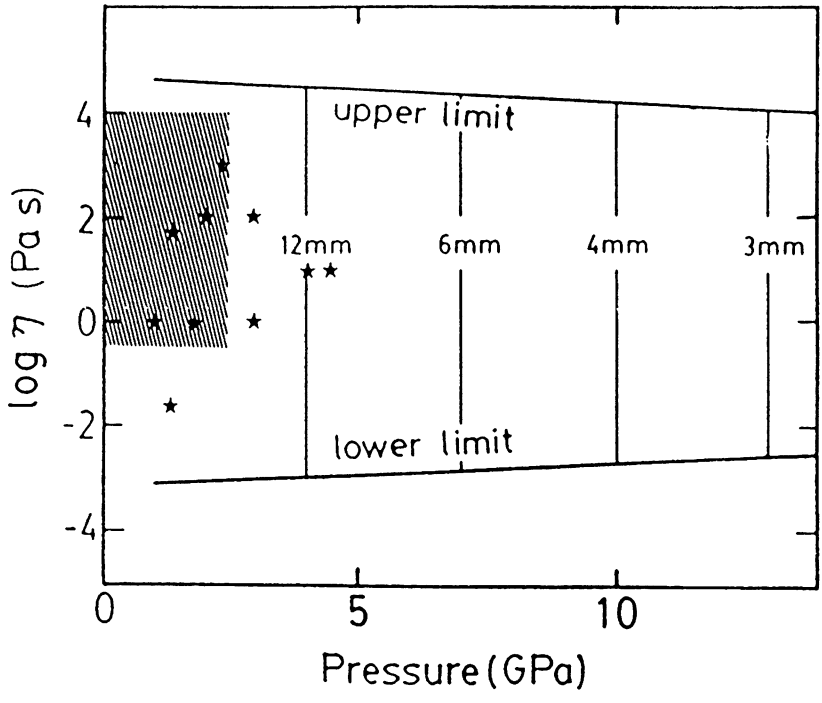

Figure 5.6. Measurable range of viscosity with pressure in a MAX80 press using synchrotron radiation (shaded area). Vertical lines indicate attainable pressures using various anvil sizes. (Redrawn from Kanzaki *et al.*, 1987.)

5.2.2. Frequency Domain Measurements

At frequencies much lower than the relaxation frequency, relaxed (liquid) frequency-independent behavior is expected for the volume, longitudinal and shear viscosities. At frequencies greater than the relaxation frequency, unrelaxed (glass) frequency-dependent viscosities are expected. Most ultrasonic studies of silicate melts are conducted at the high temperature (1000-1500°C) and relatively low frequency (3-22 MHz) conditions required to observe the relaxed (frequency-independent) longitudinal viscosity of the melt. In cases (*e.g.* Manghnani *et al.*, 1981 (basalt melts); Sato and Manghnani, 1985 (basalt melts); Rivers and Carmichael, 1987 (silicate melts)) where the experimental conditions were approaching the relaxation frequency of the melt, frequency-dependence of the longitudinal viscosity has been observed. In studies where the frequency of the applied signal has been greater than that of the relaxation frequency of the melt,

shear wave propagation has been observed (Tauke *et al.*, 1968 (B_2O_3); Macedo *et al.*, 1968 (Na_2O-B_2O_3-SiO_2);Webb, 1991 ($Na_2Si_2O_5$)).

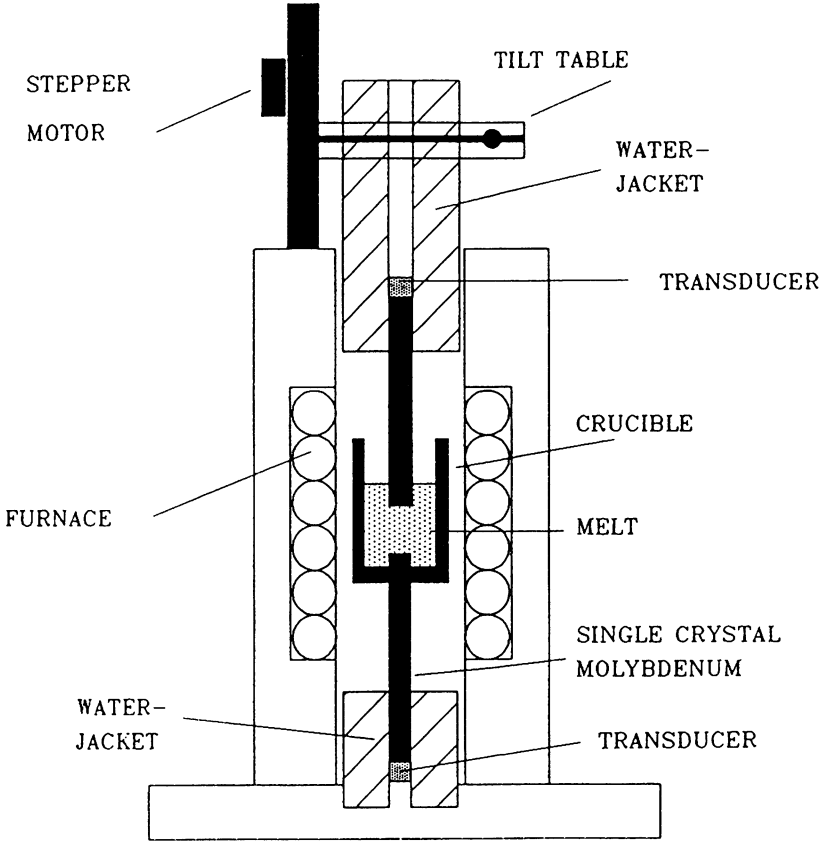

Figure 5.7. The crucible and twin buffer-rod system for determining the Newtonian and non-Newtonian behavior of silicate melts at ultrasonic frequencies.

a. Ultrasonic Attenuation

The shear and longitudinal viscosities of a melt can be determined from the velocity $c(\omega)$ and attenuation $\alpha(\omega)$ of a shear or longitudinal wave travelling through the melt; where the amplitude of the wave is

$$A(\omega,t) = A_0 \exp^{-\alpha x} \exp^{i\omega(t-x/c)} \qquad (5.10)$$

for time t, angular frequency ω (2π·frequency) and distance x (O'Connell and Budiansky, 1978). The buffer-rods are commonly single crystals of molybdenum. Small strains ($<10^{-6}$) are used and linear stress-strain theory is applicable. A shear wave begins to propagate a measurable distance (>1 wavelength) through a melt when the period of the wave is decreased to within 2 orders of magnitude more than the relaxation time of the melt structure. When the period of the shear wave is much less than the relaxation time of the melt, the wave will propagate without measurable attenuation.

For the interferometric technique of Katahara *et al.* (1981), a pulsed sinusoidal signal is transmitted from the transducer through the buffer rod and into the melt. The signal reverberates a semi-infinite number of times within the melt and is returned to the sending transducer. The amplitude of the reflected signal is monitored as the upper buffer-rod is moved (see Fig. 5.7). The amplitude of the reflected signal is;

$$|A_r|^2 = \frac{\mathcal{R}^2\left[\exp(4\alpha L) - 2\exp(2\alpha L)\cos(4\pi Lf/c) + 1\right]}{\exp(4\alpha L) - 2\mathcal{R}^2\exp(2\alpha L)\cos(4\pi Lf/c) + \mathcal{R}^4} \qquad (5.11)$$

(Rivers, 1985) where α is the attenuation coefficient, L the melt thickness, c the signal velocity and $\mathcal{R}$ is the reflection coefficient at the buffer rod-melt interface. The amplitude versus thickness data are fit to Eqn. 5.11, resulting in the calculation of velocity and attenuation of the wave. The real component of the modulus $M'(\omega) = \rho c^2$ and the imaginary component of the modulus $M''(\omega) = M'(\omega)c\alpha/\pi f$ (where the quality factor $Q = M'(\omega)/M''(\omega) = \pi f/c\alpha$; O'Connell and Budiansky, 1978) are then calculated for each temperature and frequency condition; where ρ is the melt density.

Viscosities are calculated from the velocity and attenuation data in that

$$\eta^*(\omega) = M^*(\omega)/i\omega,$$

or

$$M^*(\omega) = M'(\omega) + iM''(\omega) = M''(\omega) + i\eta'(\omega)\cdot\omega = \eta''(\omega)\cdot\omega + i\eta'(\omega)\cdot\omega \qquad (5.12)$$

and the real component of the frequency dependent viscosity is

$$\eta'(\omega) = \frac{2\rho c^3\alpha}{\omega^2}. \qquad (5.13)$$

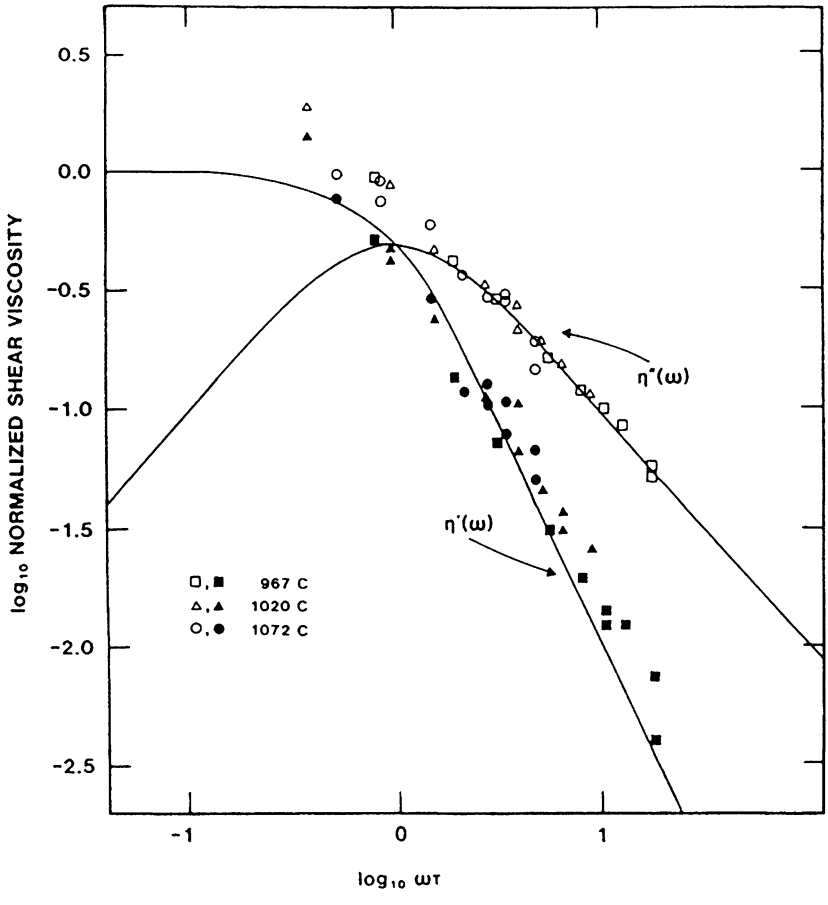

Figure 5.8. The real, $\eta'(\omega)$, and imaginary, $\eta''(\omega)$, components of the frequency dependent shear viscosity of $Na_2Si_2O_5$ melt determined using ultrasonic techniques in the frequency range 5-150 MHz at temperatures 967-1072°C. The shear viscosity has been normalized to the Newtonian shear viscosity ($10^{1.3}$-$10^{2.3}$ Pa s) at each temperature. The frequency has been normalized to the Maxwell relaxation time. (Redrawn from Webb, 1991.)

The shear viscosity (Fig. 5.8) can be calculated from the velocity and attenuation of the shear wave. The data from the propagating longitudinal wave results in the determination of the longitudinal viscosity, from which the volume viscosity can be calculated

$$\eta^*_l(\omega) = \eta^*_k(\omega) + 4\,\eta^*_s(\omega)/3\ . \qquad (5.14)$$

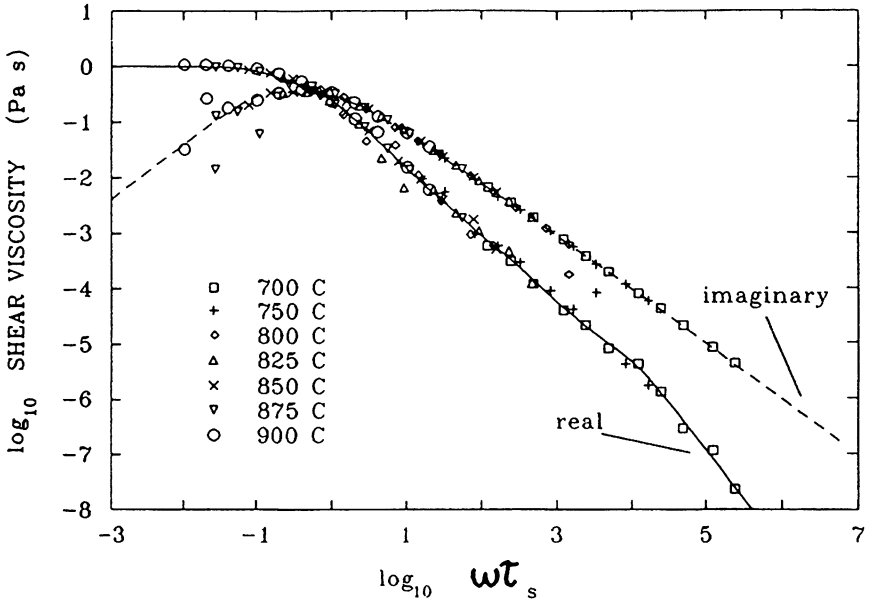

Figure 5.9. The frequency-dependent real and imaginary components of the shear viscosity of rhyolite composition melt from 700-900°C at 0.005-10 Hz. The viscosity is normalized to the Newtonian (strain-rate independent) viscosity. The frequency is normalized to the Maxwell relaxation time calculated from Eqn. 5.4. (Redrawn from Webb, 1992.)

b. Torsional Deformation

The frequency-dependence of the shear viscosity of silicate melts can be determined over a 10^{10}-10^{15} Pa s viscosity range and a 0.03-63 rad s^{-1} angular frequency range using forced torsional deformation (see Fig. 5.9). A forced oscillation apparatus is illustrated in Fig. 5.10. An 8 mm diameter cylinder of melt (25 mm long) is melted onto the two 250 mm long alumina rods at high temperature. The composite alumina-melt-alumina rod is rigidly fixed at one end. The free end is fixed to an assembly on rotational bearings. The arms of this assembly form part of an electromagnetic moving coil system. Torque is generated by the application of a sinusoidal signal (0.005-10 Hz) to the coils. Two aluminum arms are rigidly attached to the alumina rods. At the ends of these

arms are iron plates. These plates sit between pairs of capacitive pickups P1 and P2. The sinusoidal torque applied to the free end of the rod by the moving coil assembly has an amplitude of 1.5-2.5x10^{-3} N m. This results in twists of ~10^{-5} rad being observed at the two pickup points for a solid rod of alumina.

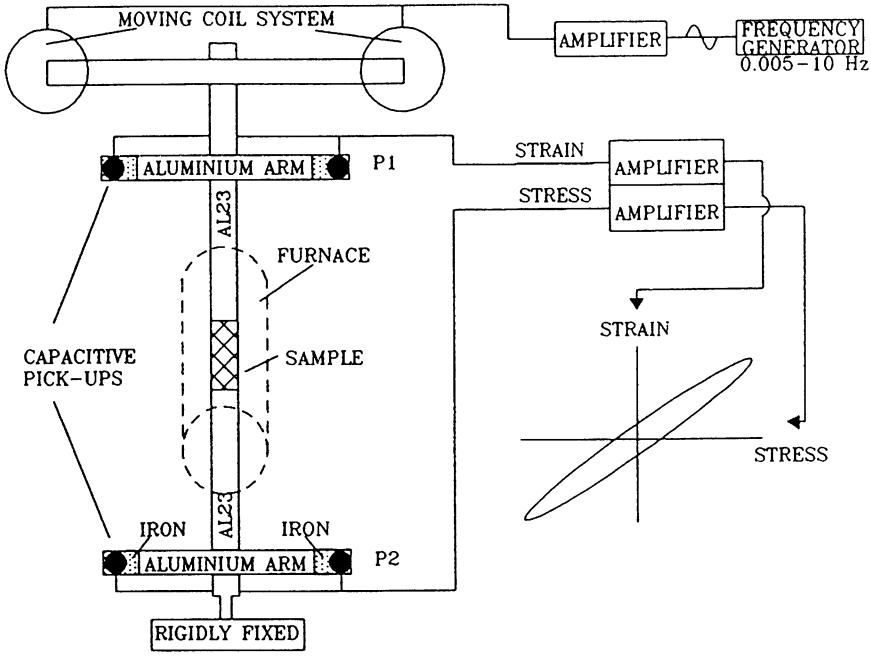

Figure 5.10. Schematic of a forced oscillation torsion apparatus. The moving coil system applies a sinusoidal stress to the sample via alumina buffer rods. The twist of the specimen is measured at P1 and P2 by the movement of iron tipped aluminium wings between pairs of capacitive transducers. The phase-shift between the applied stress and the resulting strain appears as an ellipse in a stress-strain plot. (Redrawn from Webb, 1992.)

The observed angle of twist and phase-shift between P1 and P2 is converted to an elastic component in-phase with the signal from P2 and a viscous component 90° out-of-phase with this signal. The contribution from the alumina rods is subtracted from the two components and the resulting in- and out-of-phase amplitudes are converted into an angle of twist θ and a phase-shift Ψ occurring across the melt. The shear modulus of the melt is then determined

from the applied torque C (calculated from the signal at P2), the length of the melt *l*, the radius of the melt r, and the angle of twist in the melt θ;

$$G(\omega) = \frac{2Cl}{\pi r^4 \theta(\omega)} \qquad (5.15)$$

(Avery and Ingram, 1971). Linear stress-strain behavior is observed. The frequency-dependent shear modulus determined from Eqn. 5.15 can be rewritten in terms of real and imaginary components (in-phase with the signal at P2 and 90° out-of-phase with the signal at P2) of a complex modulus;

$$G^*(\omega) = G(\omega) \cos [\psi(\omega)] + i\, G(\omega) \sin [\psi(\omega)] = G'(\omega) + i\eta'_s(\omega)\cdot\omega \,. \qquad (5.16)$$

Oscillation viscometry also records the damping of harmonic waves in a viscous medium. Tørklep and Øye (1979) and Danek *et al.* (1983) describe designs in which a torsion pendulum is constructed from a noble metal cylinder terminated with conical ends, suspended from a Pt wire, in the melt sample. This method has been used for low viscosity liquids by Danek *et al.* (1985) for the CaO-FeO-Fe_2O_3-SiO_2 system, and by Licko and Danek (1986) for the CaO-MgO-SiO_2 system in the range of 0.1 to 25 Pa s.

5.2.3 High P-T Deformation Apparatus

Most of the problems concerning the rheology of solid-liquid aggregates with low melt fractions that are relevant to crustal and mantle environments (including some brittle phenomena) involve high-temperature plastic deformation of the solid phase. Laboratory studies of plastic flow in rocks are generally restricted to experiments at high confining pressures and temperatures. The principal advant-ages of high confining pressure (≥0.3 GPa) are to (1) suppress brittle behavior (fracturing and disaggregation along grain boundaries) caused by the anisotropic thermal expansion and elastic deformation common in rock-forming minerals, and (2) attain P-T conditions which reproduce crustal and mantle conditions. This is particularly important in crystal-liquid systems and the study of geologically realistic multiphase assemblages used in the understanding of naturally occurring phase changes. In the ideal scenario, the approach used in experimental deformation should match all natural conditions. These include the presence and activities of multiple chemical species, hydrostatic pressure or mean normal stress, temperature, deviatoric stress and strain, microstructure, time and consequently the secular history of all of these

parameters. In practice it is impossible to reproduce all the conditions of crustal and mantle deformation simultaneously, and some parameters such as geologic times and/or strain-rates are not attainable experimentally. The tradeoffs are principally based on the type of problems envisaged, available experimental methods and expertise. Because of the importance of experimental design many types of instruments are commonly used in the deformation of solid-liquid systems.

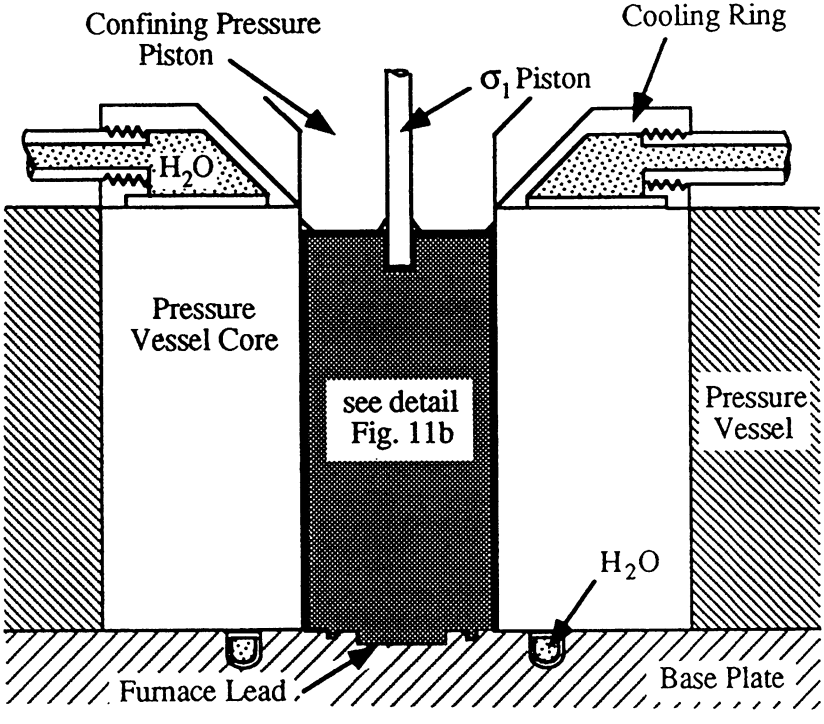

Figure 5.11. (a) Schematic diagram of solid medium assembly in pressure vessel for the Griggs-Blacic piston cylinder type solid medium deformation apparatus. The confining pressure is applied to the sample by a steel piston via a lead disc at the top of the sample assembly. The axial stress is applied to the sample by advancing a small tungsten carbide piston (σ_1 piston) coaxial with the confining pressure piston. The sample assembly and pressure vessel are water cooled by circulating top and bottom through brass and copper tubes (H_2O).

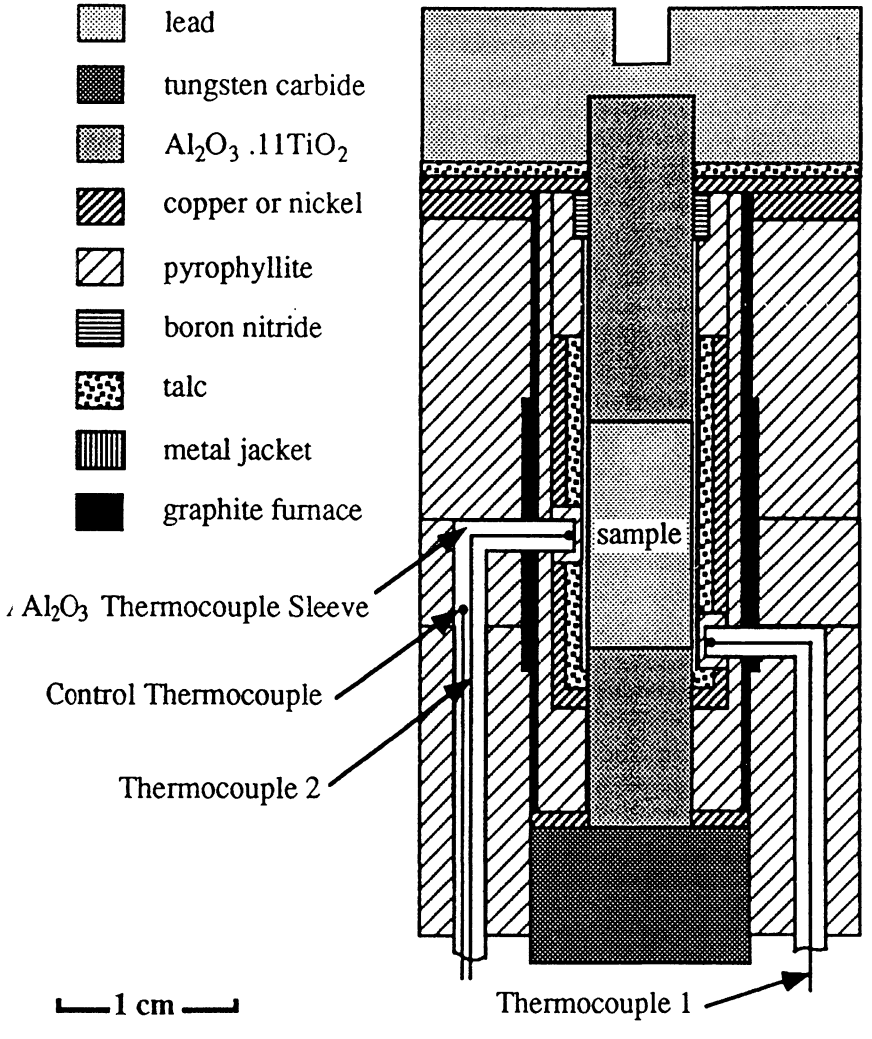

Figure 5.11. (b) Modified solid medium deformation assembly (Bussod, 1990). Friction in this assembly is reduced principally by the addition of a boron nitride ring and metal jacket along the top ceramic end piece and the use of a 1/8" (3.2 mm) diameter tungsten carbide piston. Thermal gradients are minimized ($\Delta T<5°C$) by the presence of a stepped graphite heater and a metal slug surrounding the sample and confining medium. In this assembly the confining medium is talc which transforms into a soft crystal-liquid water-rich mixture above 800°C.

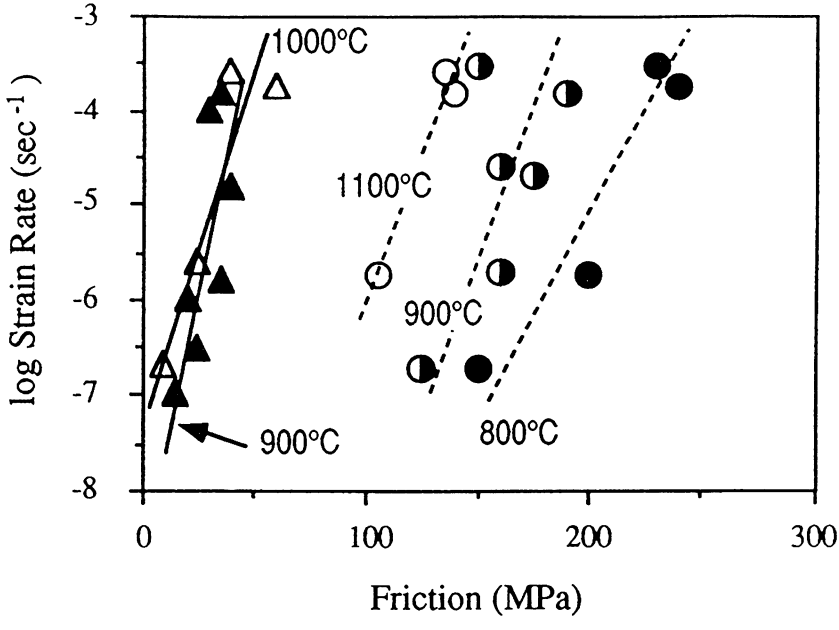

Figure 5.12. Measured friction as a function of strain-rate for the Griggs-Blacic deformation apparatus. Circles represent older deformation assembly design used in conjunction with a 1/4" (6.3 mm) load piston. Triangles represent values obtained for the modified assembly of Figure 5.11. Friction was measured using the piston in-out technique described in Koch (1983). Note the drastic reduction in friction which is virtually temperature and strain-rate independent.

One atmosphere designs are common and allow the precise determination of stress, temperature and fO_2. Because these instruments are restricted to ambient pressures, however, brittle behavior is inevitable in natural rock assemblages and their analogs, and they are mostly used in the investigation of deformation mechanisms in single crystals at low strains and/or synthetic aggregates of very small grain sizes ($\leq$10μm). These small grain sizes, however, generally favor diffusive- over dislocation-deformation mechanisms. One of the most promising deformation designs is the gas-medium apparatus which is being increasingly used in the study of rock deformation as it allows accurate measurements of flow strength under controlled temperatures and confining and pore-fluid pressures. These apparatus are internally heated, use gas as a confining medium and more importantly can be designed with an internal load cell which permits in theory, the determination of the differential stress applied to the specimen within $\pm$0.2

MPa. At this time, however, the apparatus involves several complexities associated with the containment of the high pressure gas and seals associated with electrical leads to the load cell and furnace. As a consequence, experiments cannot be sustained for long periods and experimental runs rarely exceed 5 days in duration. Furthermore, high confining pressures greater than 0.5 GPa relevant to lower crustal and mantle conditions cannot be attained. Details of gas medium and one atmosphere apparatus are given in Kohlstedt and Chopra (1987).

The only apparatus presently available for high-temperature, high pressure rock mechanics studies (which comes closest to reproducing the actual P-T conditions of the Earth's lower crust and upper mantle) is the solid medium apparatus. The other principal advantage of solid-medium piston cylinder-type apparatus is their long term stability at high P-T conditions (>1 month), which allows chemical re-equilibration in most natural solid-liquid assemblages. Of these, the most commonly used, is the Griggs-Blacic apparatus, originally designed by D.T. Griggs and co-workers in the early 1960's in which deformation tests are commonly performed at 1.5 GPa confining pressure. Other solid medium designs have extended the maximum pressure range to 3 GPa (Green and Borsch, 1990), and recent modifications in multi-anvil assemblies allow deformation tests to be performed at pressures of at least 16 GPa, which correspond to depths of 450 km (Bussod *et al.*, 1992). Unlike the one-atmosphere and gas-medium apparatus, the Griggs-Blacic apparatus has a relatively poor stress resolution principally due to the location of the load cell, which as a consequence of being external to the confined area measures the friction of the entire load column. As a consequence, the differential stresses measured in this apparatus include force (load) measurement inaccuracies. In practice, however, the external load cell is accurate within 0.2% and calibration of the cell and direct determination of the friction compensate for frictional errors outside the pressure vessel and eliminate most load piston confining pressure piston and sample assembly effects. In particular, recent modifications in the sample assembly (Fig. 5.11a,b) have reduced the friction between the upper ceramic endpiece and the confining material such that for modern configurations, the frictional effects sum to 50 MPa at most (Fig. 5.12). Lower frictions have been obtained in salt cells, however, the stability of these assemblies is greatly affected by the corrosiveness of the confining medium. Another recent improvement in the new assembly design is a reduction of the longitudinal and radial thermal gradient to ±5°C at 1000°C over the entire length (13mm) and width (6mm) of the specimen cylinder. For the assembly presented in Fig. 5.11b, the fO_2 is in the vicinity of the Ni-NiO buffer at 900-1000°C in the presence of a lherzolite specimen (Bussod and Christie, 1991).

Broad experience indicates that, to a first approximation, the rates of deformation and diffusion processes increase with increasing temperature so that geologically slower strain-rates may be simulated by increasing temperature. This is evident in the similarity in microstructures and textures between natural quartz mylonites and peridotites and experimentally deformed samples of the same mineralogy. There exist, however, limits to this equivalence. Bai *et al.* (1991) have shown that different competing microstructural deformation mechanisms are dominant over different temperature ranges. The important point is that there exists no apparatus capable of reproducing exact geologic lower crustal and mantle conditions where strain-rates and flow stresses are 10^{-10}-10^{-16} s^{-1} and 100-0.1 MPa respectively. Given these considerations the Griggs-Blacic solid medium apparatus is best suited to lower crustal and upper mantle problems in the temperature range of 700 to 1350°C and 0.5 to 1.8 GPa confining pressure, where the flow stresses of natural assemblages generally exceed 50 MPa for experimentally attainable strain-rates of 10^{-4} to 10^{-7} s^{-1}.

5.3. MELT VISCOSITY

5.3.1 Temperature Dependence of Viscosity

The temperature-dependence of silicate liquid viscosity has been described using a number of different equations. The simplest form, often valid for restricted temperature intervals, is a linear dependence of the logarithm of viscosity on reciprocal temperature, *i.e.* the Arrhenius equation

$$\log_{10} \eta = \log_{10} \eta_0 + 2.303 \frac{E}{RT} \qquad (5.17)$$

where η is the viscosity at temperature T and η_0 and E are the pre-exponential factor and the activation energy, respectively. Quite often, the data obtained by a single method of investigation, over a restricted temperature or viscosity interval, are adequately described by Eqn. 5.17.

With the possible exception of SiO_2, sufficient data now exist to demonstrate that in general, silicate liquids exhibit non-Arrhenian viscosity-temperature relationships. The degree of "curvature" of the viscosity-temperature relationship, plotted as log viscosity *versus* reciprocal absolute temperature, varies greatly with chemical composition (see Richet (1984) for a summary). The temperature-dependence of non-Arrhenian data can be reproduced by adding a parameter to Eqn. 5.17 to yield

$$\log_{10} \eta = \log_{10} \eta_0 + 2.303 \frac{E}{R\,(T-T_0)} \qquad (5.18)$$

where T_0 is a constant. This empirical description of the temperature-dependence of liquid viscosity is called the Fulcher or TVF (Tammann-Vogel-Fulcher) equation (after Vogel, 1921; Fulcher, 1925a,b; Tammann and Hesse, 1926).

Angell (1984) describes the concept of strong and fragile liquids based on the extent of non-Arrhenian temperature-dependence of viscosity. This consideration is extremely important where extrapolations of viscosity to lower temperatures are performed. In general, silicate melts are strong liquids in comparison with non-silicate liquids. The extent of non-Arrhenian temperature dependence varies greatly with composition. Decreasing SiO_2 content generally leads to less Arrhenian, more fragile behavior. Additionally, the increase of pressure is likely to lead to more fragile behavior.

5.3.2. Pressure Dependence of Viscosity

The falling sphere method has been used to study high pressure viscosities of natural and synthetic silicate liquids (*e.g.* Kushiro, 1976; Fujii and Kushiro, 1977; Sharma *et al.*, 1979; Dunn and Scarfe, 1986). The pressure-dependence of anhydrous silicate liquids has been summarized by Scarfe *et al.* (1986). Figure 5.13 summarizes the pressure dependence of silicate liquid viscosities to 2 GPa. The viscosities of silicate and aluminosilicate melt compositions with relatively low NBO/T (non-bridging oxygens per tetrahedrally co-ordinated cation) values decrease with increasing pressure. In contrast the viscosities of some silicate liquids increase with increasing pressure. Two studies have investigated the pressure-dependence of silicate melt viscosities across compositional joins exhibiting both negative and positive pressure dependence of viscosity. Kushiro (1976) investigated liquids along the SiO_2-$CaAl_2O_4$ join, observing a linear pressure dependence of viscosity that changed from a negative value at mole fraction $CaAl_2O_4 = 0.15$ and 0.2, through pressure invariance at $CaAl_2O_4 = 0.33$ to a positive pressure dependence at $CaAl_2O_4$. Brearley *et al.* (1986) also observed a transition from positive to negative pressure dependence of viscosity along the join $CaMgSi_2O_6$-$NaAlSi_3O_8$. Volatile-bearing silicate liquids have been studied at high pressure by Shaw (1963), Lebedev and Khitarov (1979), Dingwell and Mysen (1985), Dingwell (1987), Brearley and Montana (1989), Persikov *et al.* (1990) and White and Montana (1990). Figure 5.14 illustrates the effects of H_2O and F_2O_{-1} on the viscosity of $NaAlSi_3O_8$ liquid.

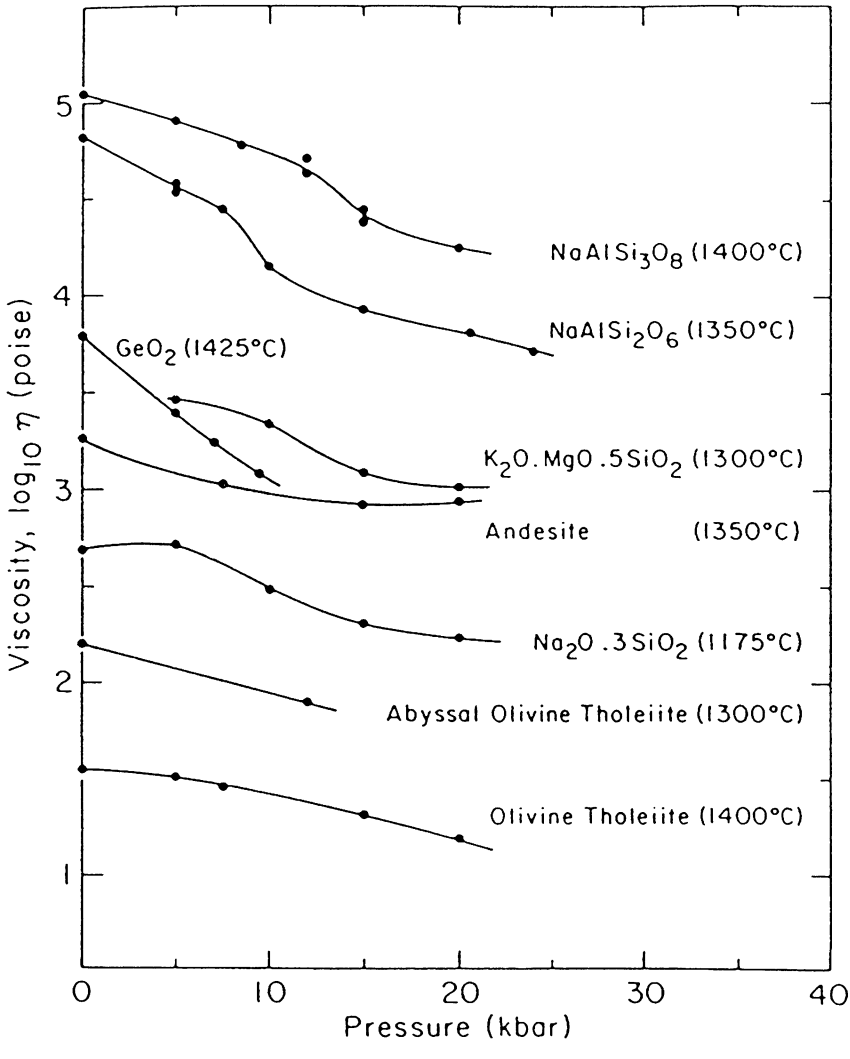

Figure 5.13. Viscosity as a function of pressure for melts. (Redrawn from Scarfe *et al.*, 1986.)

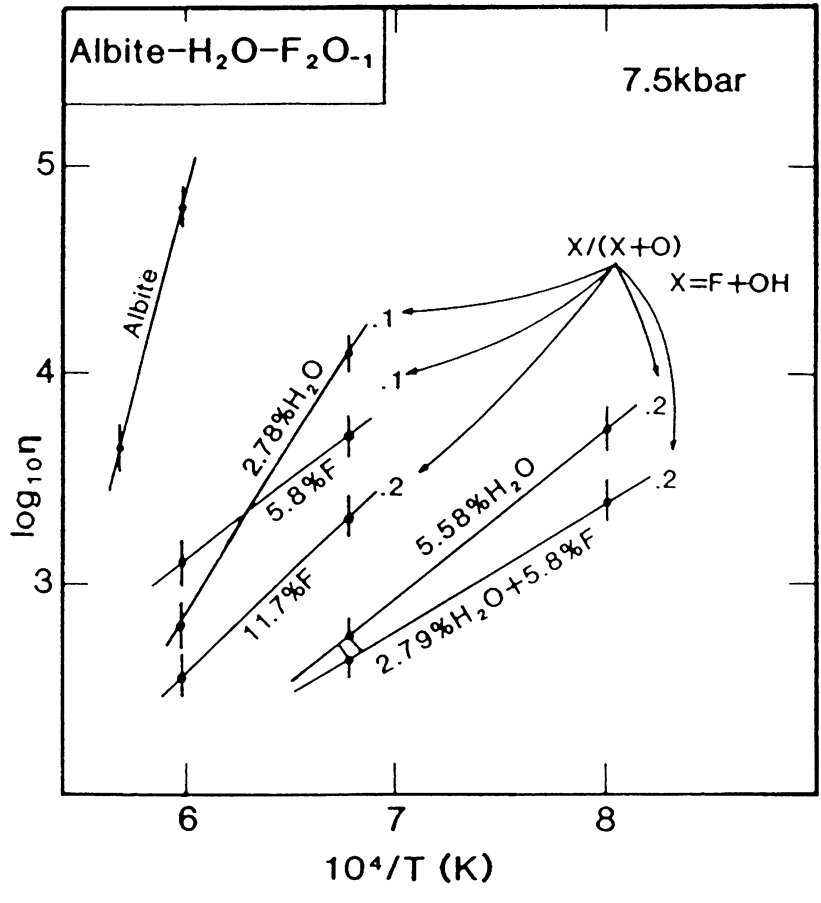

I Figure 5.14. Viscosities of melts in the system $NaAlSi_3O_8$-H_2O-F_2O_{-1} with X/(X+O) = 0.1 and 0.2 plotted versus reciprocal temperature. (Redrawn from Dingwell, 1987.)

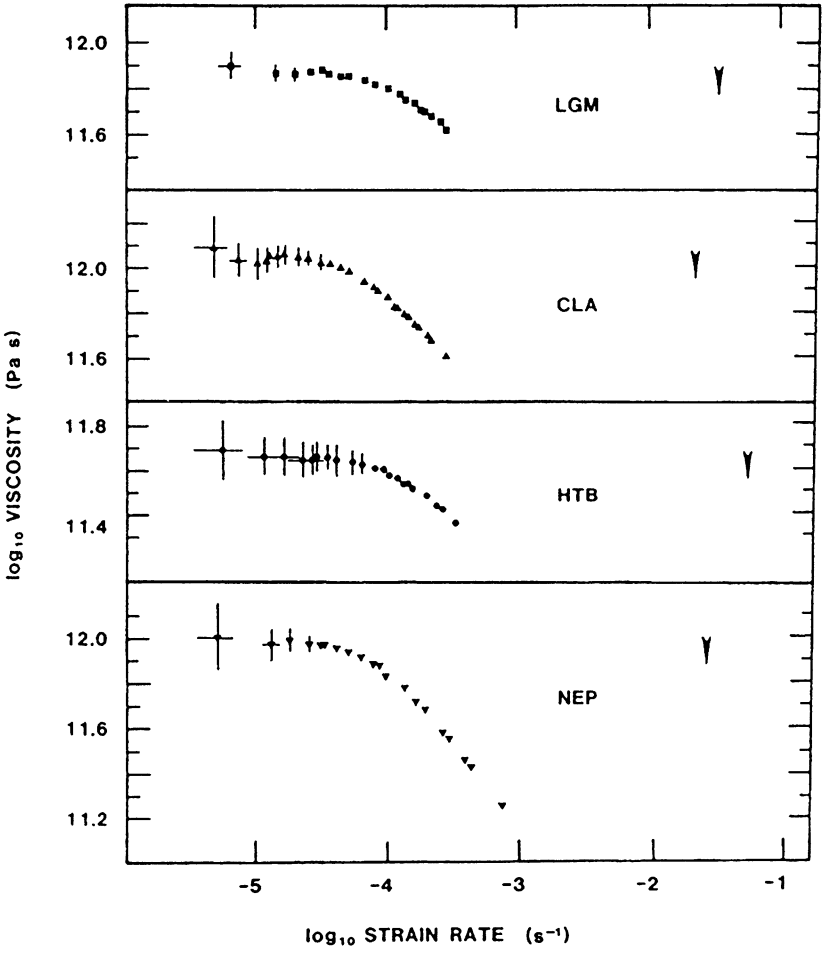

Figure 5.15. Shear viscosities for Little Glass Mountain rhyolite (LGM), Crater Lake andesite (CLA), Hawaiian tholeiite (HTB) and a nephelinite (NEP) composition melts as a function of applied strain-rate. With increasing strain-rate the onset of non-Newtonian (strain-rate dependent) behavior is observed. The arrows indicate the calculated relaxation strain-rate for these melts. (Redrawn from Webb and Dingwell, 1990a.)

5.3.3 Calculation Schemes

A number of empirical calculation schemes for the viscosity of silicate glass melts have been available for several decades (see Scholze, 1988) but calculation methods for geological melts are a more recent phenomenon. Bottinga and Weill (1972) produced a method for estimating melt viscosities at 1 atm pressure based on literature data for synthetic melt compositions. Shaw (1972) included water in his calculation model and with that allowed for the calculation of granitic melt viscosities at low pressures. No intrinsic pressure dependence of viscosity was included.

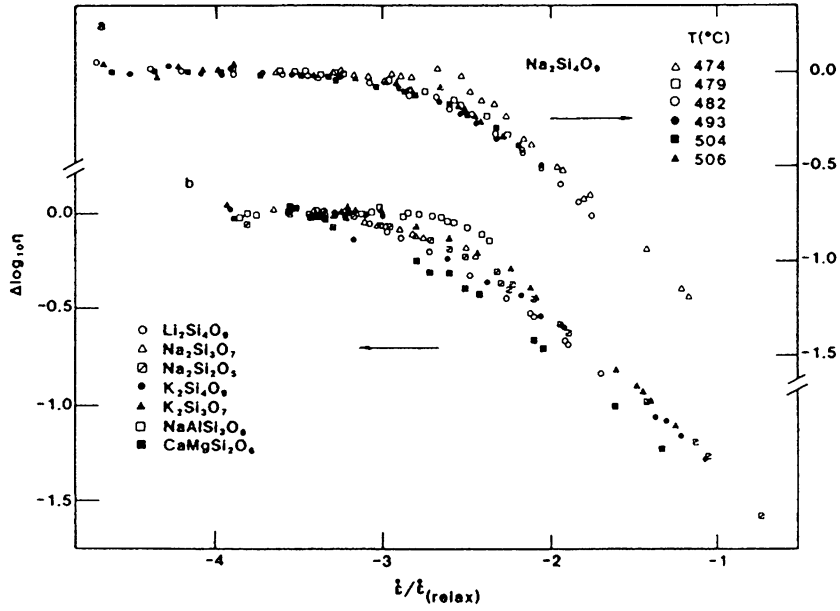

Figure 5.16. a. A reduced plot of shear viscosity (relative to Newtonian) versus strain-rate (normalized to the relaxation strain-rate) for $Na_2Si_4O_9$ at temperatures from 474 to 506°C. b. A reduced plot of shear viscosity versus normalized strain-rate for a range of silicate melt compositions. These reduced plots (based on Eqn. 5.4) remove the temperature and composition dependence of the non-Newtonian viscosity of silicate melts. (Redrawn from Webb and Dingwell, 1990b.)

5.3.4. Non-Newtonian Melt Viscosity

The Newtonian viscosity of silicate melts is a low strain-rate limiting case. With increasing strain-rate the viscosity of silicate melts eventually becomes strain-rate dependent as the value of the inverse of the strain-rate ($\dot{\varepsilon}^{-1}$) approaches the relaxation time (τ) of the silicate melt structure. This is the direct consequence of the approach of the timescale of deformation to that of the relaxation mode associated with structural relaxation in the silicate melt. All available evidence points to this relaxation mode being responsible for the onset of non-Newtonian rheology in silicate melts.

The onset of non-Newtonian viscosity has been extensively investigated by Webb and Dingwell (1990a,b). The onset of non-Newtonian viscosity for four geological melts (a rhyolite, an andesite, a basalt and a nephelinite) is illustrated in Fig. 5.15. The low strain-rate limit of Newtonian viscosity is observable below strain-rates of 10^{-4} s^{-1} whereas *shear thinning* - a decrease in viscosity with increasing shear-rate, sets in at higher strain-rates. The onset of non-Newtonian viscosity occurs approximately 3 $\log_{10}$ units of time "above" the relaxation time of each silicate melt approximated from the Maxwell relation. A normalization of the data for several compositions and at several temperatures is illustrated in Fig. 5.16 where the viscosities are normalized to the low strain-rate limiting value of Newtonian viscosity and the strain-rate of the experiment is normalized to the relaxation frequency, the inverse of the relaxation time calculated from the Maxwell relation for each melt. The composition-dependence of the onset of non-Newtonian viscosity can be removed in large part through this normalization. The success of this normalization indicates that the onset of non-Newtonian melt rheology in silicate melts can be easily estimated from Fig. 5.3, using values for the Newtonian viscosity and the shear modulus.

In addition to the effects of temperature, pressure and strain-rate on the viscosity of silicate melts, the presence of added phases (crystals and bubbles) can change the relaxation time of the melt. For the rheology of magmatic systems this case is of particular importance wherever the distribution or form of the second phase evolves during the viscous deformation of the magma.

5.4. MULTI-PHASE SYSTEMS

When a magma becomes supersaturated in volatiles by superheating or decompression, gas exsolves into spontaneously nucleated bubbles and the magmatic liquid becomes a disperse system. Cooling, which accompanies the

gas exsolution processes, as well as heat transfer from magma to country rocks causes the partial crystallization of the melt. During shear flow, such a system of silicate melt with vesicles and crystals might exhibit a wide variety of non-Newtonian effects including:

- yield phenomena ($\eta \sim (\sigma - \sigma_0)/\dot{\varepsilon}$, (where σ_0 is the stress corresponding to the transition from elastic to plastic deformation);
- pseudoplasticity ($\eta \sim \dot{\varepsilon}^{n-1}$ or shear-thinning if $n<1$ which means a decrease of apparent viscosity with increasing shear-rate, or shear thickening when $n>1$);
- non-zero primary (N_1) and secondary (N_2) stress differences (1 stands for the direction of flow, 2 stands for the direction of the shear gradient);
- rheological dilatancy (an increase of volume caused by shear deformation);
- thixotropy (time effects on viscosity or a decrease of the apparent viscosity under constant shear stress or shear-rate, followed by a gradual recovery when the stress or shear-rate is reduced);
- viscoelasticity (strain-rate effects on viscous and elastic properties), (Spera *et al.*, 1988; Barnes *et al.*,1989).

The review of rheological properties of geological multiphase systems can be subdivided in three sections;

- rheology of magmatic suspensions (melt+crystals);
- rheology of magmatic melts with exsolved volatiles (melt+bubbles);
- rheology of partially melted solids (small volume fraction of melt).

Table 5.1. Notation

η, η_s	-	shear viscosity of melt
η_o	-	pre-exponential factor
η_v	-	volume viscosity of melt
η_l	-	longitudinal viscosity
$\widetilde{\eta}_s$	-	shear viscosity of emulsion or suspension
$\eta_r = \widetilde{\eta}_s / \eta_s$	-	relative shear viscosity of emulsion or suspension
$\widetilde{\eta}_s(0)$	-	shear viscosity of emulsion or suspension at zero strain-rate, or relaxed viscosity
$\widetilde{\eta}_s(\infty)$	-	shear viscosity of emulsion or suspension at high strain-rate
$\widetilde{\eta}_v$	-	volume viscosity of emulsion or suspension
η_{elong}	-	elongational viscosity

5.4.1. Rheology of Magmatic Suspensions

Suspensions can be subdivided in two classes according to their rheology: one where there are no interparticle effects; and one, where the particles build long range "structures" as a result of forces between them. This subdivision depends on the viscosity of the liquid phase and the concentration, form, and size-distribution of the particles. The long-range (colloidal) effects are important in highly concentrated suspensions where the viscosity of the interfacial liquid is less than 10^2 Pa s (Metzner, 1985). For magmas, this might be the case for basaltic melts with crystals, in the stagnant bottom layers in mafic magma chambers. In felsic magmas where melt viscosity exceeds 10^3 Pa s these "structures" of suspended crystals are improbable. Rheological properties of concentrated suspensions can be summarized as follows:

The Einstein and Einstein-Roscoe equations

$$\eta_r = 1 + 2.5\, f \tag{5.19a}$$

$$\eta_r = \left(1 - \frac{f}{f_m}\right)^{-2.5} \tag{5.19b}$$

represent accurately the behavior of suspensions over very small ranges of solid concentrations (volume fraction $f<0.1$ and <0.3, respectively) (Einstein, 1911; Roscoe, 1952). When the concentration level of solid particles is close to the dense packing (f_m), there is insufficient fluid in the flow to lubricate motion of the particles and the relative viscosity increases to infinity (Metzner, 1985).

The relative viscosity of a suspension of smooth spheres is independent of their absolute size but is dependent on their size distribution (Ward and Whitmore, 1950a). In the case of particles of irregular form the relative viscosity increases (at all concentrations) as the particle size is reduced. This is due to an increase of the volume of liquid held in the irregularities of their surfaces (Ward and Whitmore, 1950b). Thus, the increase in the shear viscosities of concentrated suspensions arises both from the presence of the particles in the liquid and immobile liquid held in the irregularities of the particle surfaces (increasing the effective volume concentration of the suspened paticles).

For uniform size suspensions the recommended expressions for relative shear viscosity are:

$$\eta_r = \frac{9}{8} \frac{\left(\frac{f}{f_m}\right)^{\frac{1}{3}}}{1 - \left(\frac{f}{f_m}\right)^{\frac{1}{3}}} \tag{5.20}$$

theoretically derived by Frankel and Acrivos (1970), or empirical relationships such as that of Thomas

$$\eta_r = 1 + 2.5\, f + 10.05\, f^2 + 0.00273 \exp(16.6\, f) \quad , \tag{5.21}$$

the Mooney equation

$$\eta_r = 2.5 \frac{f}{\left[1 - \frac{f}{f_m}\right]} \quad , \tag{5.22}$$

or the empirical expression of Maron and Pierce

$$\eta_r = \left[1 - \frac{f}{f_m}\right]^{-2} \tag{5.23}$$

(see Metzner, 1985; Utracki, 1988) all of which fit reasonably well the experimental data on the rheology of hard-sphere suspensions near the glass transition (Marshall and Zukovski, 1990). Sherman (1968), however, observed a dependence of viscosity on the size of the solid particles and describes the apparent viscosity of a suspension by

$$\log_{10} \eta_r = 0.011 \frac{D_p}{\left[\left(\frac{f_m}{f} - 1\right)^{\frac{1}{3}} - 1\right]} - 0.15 \tag{5.24}$$

where D_p is the mean diameter (in μm) of particles in suspension.

Equations 5.19-5.24 apply to the relaxed shear viscosity; the viscosity at small strain-rates in comparison with the characteristic relaxation time of the melt. The only available laboratory data on viscosities of picritic magmas at subliquidus temperatures fit the Einstein-Roscoe relationship (Ryerson *et al.*, 1988). Eqn. 5.23 has been used in calculations of pseudotachylite magmas (Spray, 1993). Some applications, however, of the above mentioned expressions

for the apparent viscosity of suspensions relative to the rheology of lavas have encountered serious difficulties. Natural magmas exhibit a much higher viscosity than that predicted by Eqns. 5.19-5.24 (McBirney, and Murase, 1984), and thus, the numerical constants involved in Eqn. 5.19 and Eqn. 5.24 have been modified in order to fit the field observations of magma rheology (Marsh, 1981; Murase *et al.*, 1985). A procedure to evaluate the viscosity of magmas based on the calculated viscosity of silicate melts (Shaw, 1972) combined with the relationship between apparent viscosity and crystallinity (Eqn. 5.24) has been proposed by McBirney and Murase (1984) and Frost and Lindsay (1988).

The parameter f_m, the critical concentration of particles (close to dense packing) varies over the range 0.52-0.74 depending on the structure, type of packing and size-distribution (Utracki, 1988). The theoretical value of f_m for hexagonal close-packing of a uniform suspension of hard spheres is f_m~0.74; experimental results on random-loose and random-dense packing give f_m~0.59-0.64 with the most probable random packing ~0.62. With an increase in the particle diameter ratio (R_{min}/R_{max}) from 1 to 10 the dense packing concentration f_m increases from 0.62 to 0.84 (*i.e.* Dabak and Yucel, 1986). The estimation of the parameter of crystal dense packing for lavas based on phenocryst statistics gives f_m~0.6 (Marsh, 1981).

The distribution of particle sizes has little effect on the relative suspension viscosity when the volume fraction of particles is below 20% (Evenson *et al.*, 1951). Near-dense packing when a very high solid concentration can be achieved (Metzner, 1985) shows an abrupt increase of apparent viscosity. The effect of particle distribution results in relative viscosity as follows:

$$\eta_r = \left[1 + 0.75 \frac{\frac{f}{f_m}}{\left[1 - \frac{f}{f_m}\right]} \right]^2 \qquad (5.25)$$

where f_m is a function of particle size distribution (Chong *et al.*, 1971) or a modified Mooney equation (Sweeny and Geckler, 1954). For a monodisperse suspension the viscosity approaches infinity at f_m~0.605. With increase of the relative volume fraction of smaller particle sizes f_m increases. The apparent viscosity of a bimodal suspension decreases when the packing of smaller particles into the interstices of the larger spheres increases (Sweeny and Geckler, 1954). Calculating f_m from the particle-size distribution (*e.g.* Dabak and Yucel, 1986) the relative viscosity of a suspension can be calculated using Eqn. 5.25. The anisotropic shape of particles leads to a f_m decrease and a relative viscosity

increase (Metzner, 1985; Utracki, 1988).

Depending on shear-rate the behavior of highly concentrated suspensions can be separated into three regions:

- a low shear-rate region where interparticle forces are dominant;
- an intermediate shear-rate region where flow is pseudoplastic;
- a high shear-rate region where the behavior is Newtonian exhibiting aligned particle movement (Dabak and Yucel, 1986).

In order to describe the behavior of the relative viscosity in all three regions the empirical expression has been proposed:

$$\eta_r(\dot{\varepsilon}) = \left[1 + A \frac{\frac{f}{f_m}}{n(\dot{\varepsilon})\left[1 - \frac{f}{f_m}\right]} \right]^{n(\dot{\varepsilon})} \tag{5.26}$$

where the parameter n depends on the strain-rate (at high strain-rate n=2) and is meant to be estimated empirically. The parameter A is a shape factor - for smooth particles A=2.5, for irregular particles A is uncertain. The parameter f_m can be calculated from the size-distribution of solid particles (Dabak and Yucel, 1986).

In highly concentrated suspensions the yield stress σ_o required to initiate flow correlates with particle size D_p and the dense packing parameter f_m via an empirical expression

$$\sigma_0 = 1.26\, \rho g \frac{D_p \left[\frac{f_m}{(1 - f_m)}\right]^2}{(f_m - f)\, \xi^{1.5}\, s^2} \tag{5.27}$$

where the shape factor ξ is the ratio of the surface area of a sphere of equivalent volume to the surface area of the particle, the geometric standard deviation (s) is determined from the size distribution (cumulative proportion of particles <50% size)/(cumulative proportion of particles <15.87% size) and g is the acceleration due to gravity (Gay *et al.*, 1969; Pinkerton and Stevenson, 1992). Based on experiments with flow of highly concentrated suspensions through a tube, an empirical expression for strain-rate dependent rheology has been proposed

$$\tilde{\eta}_s(\varepsilon) = \tilde{\eta}_s(\infty) + \frac{\tilde{\eta}_s(0) - \tilde{\eta}_s(\infty)}{1 + \frac{[\tilde{\eta}_s(0) - \tilde{\eta}_s(\infty)]\,\dot{\varepsilon}}{B}} \tag{5.28}$$

$\tilde{\eta}_s(0)$ is estimated from Eqn. 5.20, f_m from the size-distribution of particles,

$$\frac{B}{\sigma_0} = 0.066 \frac{f_m^2}{(f_m - f)} \left[\frac{\eta_s^2}{D_p^2 \rho \sigma_0} \right]^{0.21} \tag{5.29}$$

$$\tilde{\eta}_s(\infty) = \eta_s \exp\left\{ \left[2.5 + \left(\frac{f}{(f_m - f)} \right)^n \right] \frac{f}{f_m} \right\} \tag{5.30}$$

where n=0.48 has been determined empirically, the constant B is the shear stress factor for particle motion and is equal to the shear stress needed to overcome particle-particle interaction at high strain-rate (Gay *et al.*, 1969). The application of Eqns. 5.27-5.30 to evaluate viscosity and yield strength of natural lavas from Mount Etna and Hawaii, depending on the degree of crystallization, gives excellent results (Pinkerton and Stevenson, 1992).

Field observations of magma rheology indicate that the tholeiite charged with crystals in the Makaopuhi lava lake (Shaw *et al.*, 1968) was pseudoplastic with a yield strength 70-120 N m^{-2}. The Etna lava had a yield strength 370±30 N m^{-2} (Pinkerton and Sparks, 1978). Basaltic lavas have been estimated to have a Bingham rheology with a yield strength $9\pm2 \times 10^3$ N m^{-2} using the size of the gradient-free zone of the lava flow (Panov *et al.*, 1985). Finally, a laboratory study of partially crystallized melt revealed a relationship between the yield strength σ_o (in N m^{-2}) and the volume fraction of crystals f:

$$\sigma_0 \approx 6500\, f^{2.85} \tag{5.31}$$

resulting in $\sigma_o \sim 800$ N m^{-2} at 1140°C (Ryerson *et al.*, 1988), close to the expression $\sigma_o \sim f^3$ obtained experimentally for clay suspensions (Zhaohui, 1982).

5.4.2. Rheology of magmatic melts with exsolved volatiles

Important dimensionless parameters governing the behavior of bubble (b) - melt (s) mixtures are

$$\lambda = \frac{\eta_b}{\eta_s} \tag{5.32}$$

the viscosity ratio of disperse (vapor) and continuous (melt) phases, and the capillary number,

$$Ca = \frac{\dot{\varepsilon}\eta_s R_b}{\alpha} \tag{5.33}$$

where α i the melt-vapor interfacial tension, $\dot{\varepsilon}$ is the strain-rate, R_b is the bubble radius. Rearranging Eqn. 5.33, one obtains:

$$\tau_b \approx \frac{\eta_s R_b}{\alpha} \tag{5.34}$$

which has he dimension of time, and characterizes the relaxation time of the bubble geometry following a change in the stress field.

a. Dilute Magmatic Emulsions

The visosity of magma with bubbles has been addressed both theoretically (Shimozuru, 1978) and based on the viscosity of a liquid with spherical obstacles (Taylor, 1932; Sibree, 1934). The rheological investigation of dilute magmatic emulsions has begun quite recently (Spera *et al.*, 1988; Stein and Spera, 1992). For a dilute emulsion which (at moderate stresses) can be represented by a Newtonianliquid with spherical inclusions (f<10 vol.%) the main results may be summarzed as follows.

If an inompressible Newtonian fluid contains bubbles the suspension has a volume viscosity

$$\tilde{\eta}_V = \frac{4\,\eta_S (1 - f)}{3f} \tag{5.35}$$

(Prud'homme and Bird, 1978), where f now represents the volume fraction of porosity orbubbles.

Depending on the total strain and strain-rate of the shear flow, the behavior of bubbles may be distinguished as non-deformable, deformable and highly deformable (bubble break-up). The main features of bubble deformation and break-up have been summarized in Stein and Spera (1992).

With λdecrease ($\lambda \rightarrow 0$) the critical capillary number $Ca_{cr}(\lambda)$ at which

bubbles begin to break up, increases. For weak flows (Ca<0.4) the number of daughter droplets increases with an increase in the ratio Ca/Ca_{cr}. At strain-rates below the critical capillary number $Ca_{cr}(\lambda)$ fragmentation can occur caused by another mechanism known as "tip streaming instability" (Buckmaster, 1972). The origin of this type of instability depends on the history of the flow, especially the time rate of change of the shear strain-rate. For strong flows (very low λ) bubbles can become highly elongated before fragmentation. This is often the case during the flow of vesicular obsidians.

In experiments with dilute emulsions (f<<1) of inviscid bubbles in melts, shear viscosity increases with bubble content and exhibits a power law dependence

$$\eta_r(f) = \frac{\tilde{\eta}_s}{\eta_s} = 1 + 13.1\ f$$

$$\tilde{\eta}_s(\dot{\varepsilon}) = m\ \dot{\varepsilon}^{n-1} \qquad (5.36)$$

in the strain-rate range $\dot{\varepsilon}$~0.06-7 s^{-1} and capillary number Ca~0.5-110 with power law index n~0.87-0.93 (Stein and Spera, 1992).

The presence of slightly deformed bubbles in Newtonian liquids results in non-linear effects, such as additional characteristic relaxation times and a normal stress difference (Schowalter, 1978; Stein and Spera, 1992). The resistance to bubble deformation provided by interfacial tension results in an elastic component of the response of the emulsion to shear (Schowalter *et al.*, 1968; Frankel and Acrivos, 1970). In a laminar shear flow the normal components of stress are affected by deformation of bubbles. The first and the second normal stress differences become non-zero as for a non-Newtonian liquid:

$$N_1 \approx N_2 \approx \frac{\eta_s^2\ R_b\ \dot{\varepsilon} f}{\alpha}\ . \qquad (5.37)$$

Experimental data from rotational viscometry of magmatic emulsions show that the first normal stress differences, N_1~2% of the shear stress, and for the conditions relevant to magma flow they can be as great as 25-40% of the shear stress (Stein and Spera, 1992).

The dependence of viscosity on porosity or bubble content (f) in melts and highly viscous liquids ($\tilde{\eta}_s > 10^9$ Pa s) differs from Eqn. 5.35 or 5.36. Theoretical analysis and experimental testing of different relationships between viscosity and porosity of melts (Sura and Panda, 1990) illustrate the decrease of melt viscosity

with porosity increase. McKenzie's (1950) analysis of dilute pores results in a relative viscosity dependence (η_r) *versus* porosity (f) of

$$\eta_r = (1 - C\,f) \tag{5.38}$$

which is valid at low porosity (f<<1). A more complicated expression (Sura and Panda, 1990) derived by using the viscous analogy of elastic stresses which includes a shape factor for pores (Ω) is

$$\eta_r = \frac{3\Omega(1 - f)^2}{3\Omega(1 - f) + 2f}. \tag{5.39}$$

For spherical pores Ω = 1 and $\Omega \rightarrow 0$ when pores totally surround solid particles. In the case of spherical non-interacting inclusions at low porosities the dependence of viscosity on volume fraction of bubbles should be linear as in Eqn. 5.38 and at high porosities (f>0.5) as demonstrated experimentally (Sura and Panda, 1990) $\eta_r \approx 1/f$. In order to reconcile these two conditions it is reasonable to fit the experimental data of viscosity *versus* porosity to a relationship such as

$$\eta_r(f) = \frac{1}{1 + Cf} \tag{5.40}$$

which has a linear approximation (Eqn. 5.38) at small porosity ($f \rightarrow 0$).

In parallel plate experiments with vesicular highly viscous melts ($\lambda \approx 10^{-14}$ to 10^{-16}) at small strains (10^{-3}) and strain-rates 10^{-5} to 10^{-7} s^{-1} the shear viscosity decreases with volume fraction of bubbles (Bagdassarov and Dingwell, 1992):

$$\eta_r(f) = \frac{1}{(1 + 22.4\,f)}. \tag{5.41}$$

In the case of $\lambda \ll 10^{-10}$ the decrease of the viscosity of a melt+bubble mixture is expected at strain-rates much smaller than the inverse of the bubble's relaxation time t_b^{-1} (or $\dot{\varepsilon}\tau_b << 1$). In this case the stress analysis for the suspension can be obtained from the stress analysis of an elastic material by the viscous analogy (*e.g.* Sura and Panda, 1990). Accordingly, the elastic shear modulus G of a porous material is replaced by the shear viscosity, and the elastic bulk modulus K is replaced by the volume viscosity.

The experimental data on vesicular rhyolite melt indicate that the apparent

compressional viscosity measured in vesicular samples decreases by an order of magnitude with a porosity increase of 25 % and then remains constant (see Fig. 5.17). At low porosity the deformation character of samples indicates practically incompressible behavior. This means that the measured viscosity is elongational (η_{elong}) and relates to the shear (η_s) and volume (η_v) viscosity of the material via Eqn. 5.3.

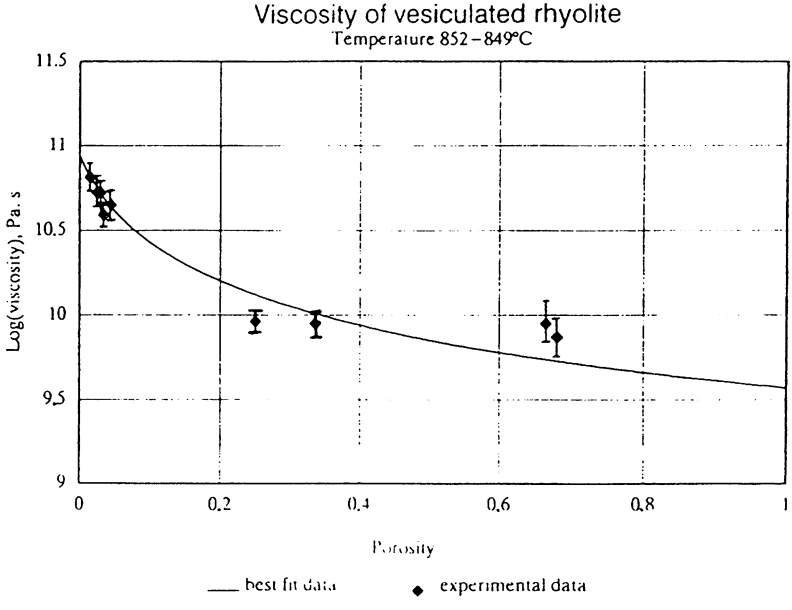

Figure 5.17. Viscosity of vesicular rhyolite melts as a function of porosity. (Redrawn from Bagdassarov and Dingwell, 1992.)

At high porosity, the character of sample deformation indicates pure uniaxial compression and in this case the measured viscosity is longitudinal and relates to shear and volume viscosity via Eqn. 5.3. Dynamic viscosity measurements using a forced oscillation technique have also demonstrated a decrease of the relaxed shear viscosity of rhyolite melt with increasing porosity (Bagdassarov and Dingwell, 1993a).

b. Rheology of Magmatic Foam

The main results from rheological studies of foams (f>0.75) have been recently reviewed by Kraynik (1988) and may be summarized as follows.

Diffusion processes in bubbles and the natural tendency of foams to diminish their surface area both favor bubble growth. This makes foams unstable under shear flow at high strain-rates. At low strain-rates there is an excellent analogy between foams and highly concentrated liquid-liquid suspensions. Foams with a high volume fraction of bubbles (>75%) are viscoplastic bodies with a yield strength which is a strong function of liquid content. There are other non-Newtonian features of foam rheology such as "slip on the wall", and changing of bubble geometry under shear flow which are important in volcanological applications but have not yet been studied for geological systems.

Experimental study of the shear stress response of bubble-bearing melts has shown a specific overshoot of stresses (see Fig. 5.18) which is typical for the rheology of two-phase media with changeable geometry of phases. The effective description of a medium with changing geometry of phases under applied stresses can be represented as a Burgers body (Fig. 5.19) with two characteristic relaxation times. A Burgers body consists of a Maxwell element (Newtonian viscous dash-pot with viscosity η_1 + Hookean elastic spring with rigidity G_1 in series) and a Kelvin element (dash-pot η_2 + elastic spring G_2 in parallel) combined in series. There are two different timescales in the shear flow of bubble-bearing melt. The first is given by $\tau_s = \eta_s/G$, the relaxation time of viscous stresses in the melt (Maxwell relaxation time, where G is the unrelaxed elastic shear modulus). The second characterizes the way in which vesicles accommodate viscous stresses through deformation (Bentley and Leal, 1986). The behavior of deformable vesicles in a time-dependent shear flow is described by the relaxation time $\tau_b = R_b \eta_s/\alpha$. For $R_b \sim 10$ mm, $\eta_s \sim 10^6$ Pa s, and $\alpha \sim 0.5$ N m^{-1} the relaxation time $\tau_b \sim 20$ sec which is consistent with the observed stress overshoot decay in Fig. 5.18. The elastic behavior results from the presence of a finite interfacial tension α which acts to oppose viscous deformation of a bubble from the spherical shape (Frankel and Acrivos, 1970). The mechanical behavior of bubble-free melts in the temperature range under consideration can be adequately described by the Maxwell body. Viscoelastic behavior of bubbles complicates the model by adding a pair of elastic and viscous elements (Fig. 5.19).

In the rotational viscometry experiments of Fig. 5.18 (Bagdassarov and Dingwell, 1993b) the response of a material under the action of an applied shear-rate has been considered. In nature this situation relates more to the shear contact zones of magma flow than to the flow of magma in a volcanic conduit under applied pressure. Inasmuch as the model of mechanical behavior is generally defined in terms of viscous and elastic elements, the creep of material under an applied stress can be predicted:

$$J(t) = \left(\frac{1}{G_1} + \frac{t}{\eta_1} + \frac{1}{G_2}\left[1 - \exp\left(-\frac{G_2 t}{\eta_2}\right)\right]\right), \tag{5.42}$$

where the compliance J relates the applied stress to the resulting strain. There are two relaxation timescales in a Burgers body, $\tau_1=\eta_1/G_1$ and $\tau_2=\eta_2/G_2$ determining the relaxation process of two elements, the viscoelastic Maxwell liquid and the anelastic Kelvin solid. The deviation from Maxwell body behavior begins when $\tau_2 \neq 0$. If τ_2 is comparable with τ_1 then the time dependence of stress relaxation will be given by

$$\sigma(t) = \eta_1\dot{\varepsilon}_0 + C_1 \exp\left(-\frac{t}{\tilde{\tau}_1}\right) + C_2 \exp\left(-\frac{t}{\tilde{\tau}_2}\right) \tag{5.43}$$

where $\tilde{\tau}_1$ and $\tilde{\tau}_2$ are functions of τ_1 and τ_2. If $\tilde{\tau}_1 > \tilde{\tau}_2$ and $C_1<0$, $C_2>0$, one obtains an overshoot on the stress-strain curve before the stress reaches the steady state value $\eta_1\dot{\varepsilon}_0$.

The noted time-dependent behavior of natural foams and vesicular melts can contribute to the magma flow at the start of stress application or to the pulsating regime of a gas-magma mixture flowing in a volcanic channel (Wilson *et al.*, 1980).

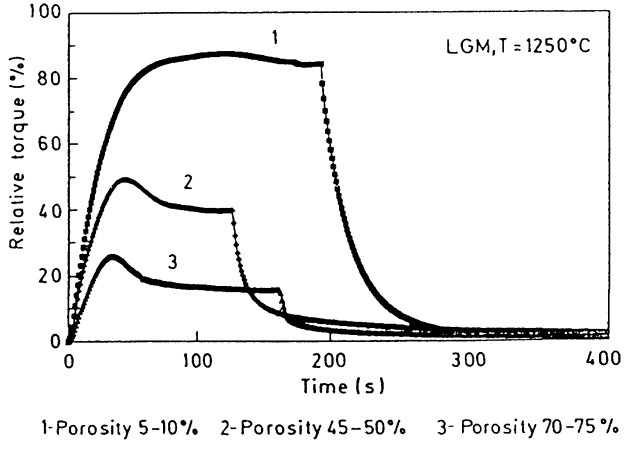

Figure 5.18. Response of bubble bearing rhyolite composition melts to an applied step function in stress, as a function of time. (Redrawn from Bagdassarov and Dingwell, 1993b.)

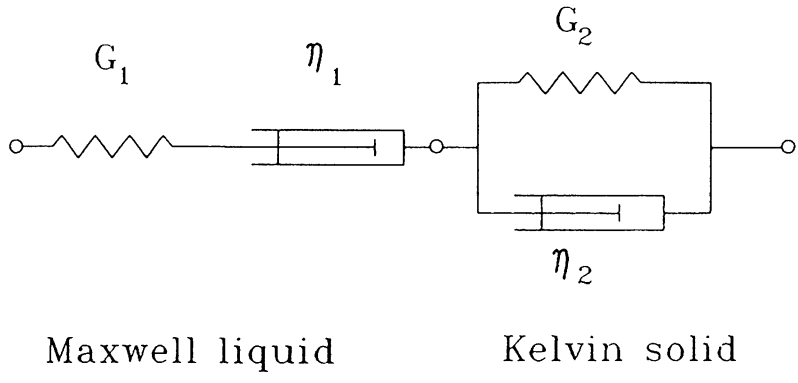

Figure 5.19. Burgers body combining a Maxwell liquid and a Kelvin solid to describe the stress-strain behavior of a linear viscoelastic material.

5.5. RHEOLOGY OF PARTIALLY MOLTEN ROCKS

Magmas can be transported by processes of diapirism, percolation, and fracturing. All of these can involve the deformation of the solid matrix and are rate-limited, at least in part, by the rheological properties of the rock. A distinction must be made between crystal-liquid aggregates with low melt fractions for which the rheologic behavior of the system is dominated by the solid phase and crystal-liquid suspensions where the flow behavior is controlled by the liquid. In rock mechanics, this corresponds to a boundary known as the RCMP or Rheological Critical Melt Percentage, defined by Arzi (1978) as the critical melt fraction for which a rock disaggregates or is "fluidized".

The response of a rock to melting and melt migration involves deformation of the crystalline matrix by compaction, simple shear and/or fracturing. In a partially molten aggregate, the solid phase acts as a skeletal framework with a porosity (melt fraction) such that for melt segregation to occur, the matrix must deform. Compaction and fracturing represent transient plastic and brittle phenomena respectively, and the deformation of a rock by simple shear at high P-T can involve steady-state dislocation and diffusion-accommodated processes. The study of each of these mechanisms involves various experimental approaches, designs and apparatus. The non-hydrostatic stress gradient related to

the flow of the matrix by pure compaction and simple shear (no compaction), is characterized by the bulk and shear viscosities, respectively (McKenzie, 1984; Scott and Stevenson, 1986). The volume or bulk viscosity relates the rate of compaction to the pressure difference between the solid and liquid phases, whereas the shear viscosity relates the steady-state flow stress of the solid framework in the presence of melt to the shear strain-rate (without compaction). From the point of view of melt segregation processes, the critical issues concerning the deformation of a rock in the presence of melt are:
i) What is the RCMP or the melt fraction at which the mechanical properties of the rock are no longer dominated by the solid matrix?,
ii) What is the rheology of a partially molten rock during compaction (bulk viscosity) and flow (shear viscosity)?,
iii) Under which conditions does melt segregation occur?

5.5.1 The RCMP

Arzi (1978) determined the change in the total effective viscosity in Westerly granite and San Marcos gabbro with controlled melt percentages of up to 17 vol.%, for applied shear stresses of 0.10 to 10 MPa, and 200 MPa water pressure. He found that for a melt fraction below 20±10 vol.% (RCMP) bulk shear and compactive filter pressing are drastically reduced requiring strains in the solid fraction and/or the deformation of very thin melt films. Using observations on melted ceramics deformed in axial compression (Allison *et al.*, 1959), and comparisons with partially melted ultramafic nodules, Arzi (1978) incorporated his results into a theoretical analysis by Einstein (1911) modified by Roscoe (1952) to extend these conclusions to mantle behavior in the presence of melt (see Fig. 5.20). Based on this analysis, Arzi concluded that spatial continuity in the solid grains due to solid grain-to-grain binding and/or interlocking, should provide resistance to deformation at low melt percentage and high confining pressures. Above the RCMP a rheological "breakdown" (drop in bulk viscosity of several orders of magnitude) is predicted even when superimposed on other gradual effects such as the softening of the solid framework, enhanced mass transfer (higher diffusivities) through the melt (Stocker and Ashby, 1973), or changes in the melt viscosity. In fact, above the RCMP at a critical melt fraction of approximately 35 vol.%, hydrostatic experiments on garnet lherzolite (Arndt, 1977) and granite (Van der Molen and Paterson, 1979) show a complete disaggregation of the solid framework and melt separation by gravitational settling at very short times (hours). Details of the initiation of this disaggregation are not well understood although observations on experimentally

deformed hypersolidus lherzolite suggest that this is related to a grain boundary sliding mechanism (Bussod and Christie, 1991). Overall the RCMP is not well defined. There is evidence that its value is strain rate-, bulk composition-, fluid pressure- and stress-dependent, which can control the melt topology or the interconnectivity of the melt phase. Experimental deformation studies on natural and synthetic mantle assemblages place the onset of the RCMP closer to 10±2 vol.% melt, corresponding to a drop in effective viscosity by a factor of 3 to 4 at low to moderate stresses (σ=50-200 MPa; Bussod and Christie, 1991).

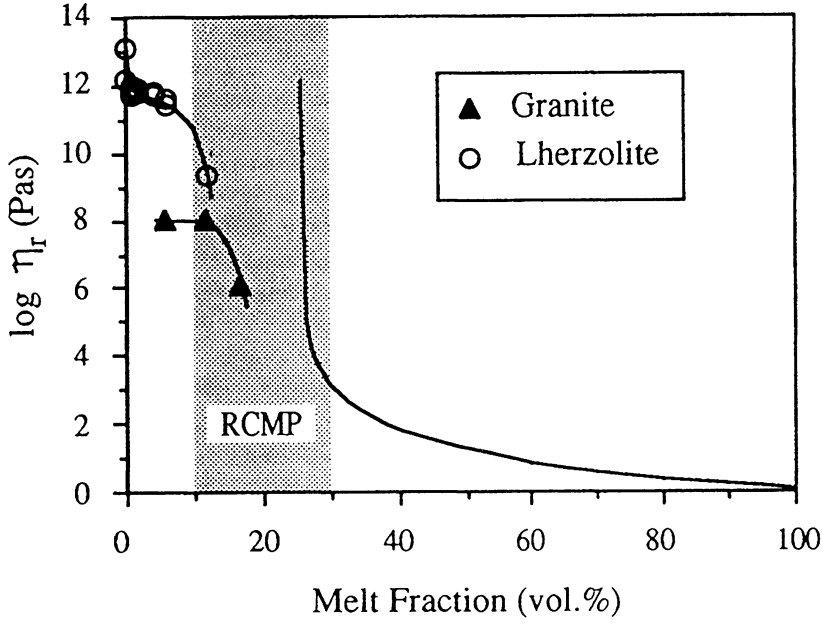

Figure 5.20. Representation of the RCMP modified from Arzi (1978). The solid curve shows the relative viscosity (ratio of volume viscosity of a crystal-liquid suspension to the viscosity of the liquid) versus the melt volume percentage for a suspension of rigid spheres according to the theory of Roscoe (1952). The solid triangles represent experimental values for Westerly granite (Arzi, 1978) and the open circles are experimental data on lherzolite using effective viscosities (Bussod, 1990). The shaded area represents the RCMP proposed by Arzi (1978).

5.5.2 Effect of Partial Melt on Rheology

Ideally, the application of a deviatoric stress to a single crystal leads to immediate elastic strain, followed by steady-state deformation, mechanically characterized by a specific strain-rate ($\dot{\varepsilon}$) for a given applied stress (σ). For such a condition and within a limited range of stress and temperature, the material property can be semi-empirically fitted to an Arrhenius type constitutive relation of the form

$$\dot{\varepsilon} = A\,\sigma^{n}\,d^{-m}\,p_{O_2}{}^{-k}\exp\left(\frac{-Q^*}{RT}\right) \qquad (5.44)$$

where the material properties are the grain size (d), the activation enthalpy for the rate limiting process (Q*), the partial pressure of oxygen (pO_2) and a material constant (A) which depends on the microstructure and composition. To a first approximation, this equation also applies to the steady state deformation of multiphase aggregates, although the significance of some of the terms is increasingly obscure as the complexity of the system increases. Furthermore when a fluid phase is present frictional mechanisms (*e.g.* grain boundary sliding) may become important and at high P-T the rheologic behavior of the material may become elastoplastic (*i.e.* recoverable + permanent deformation).

a. Compaction

Densification or compactive filter pressing in rocks has been addressed experimentally by numerous authors (Arndt, 1977; Arzi, 1978; Van der Molen and Paterson, 1979; Cooper and Kohlstedt, 1984a, 1986; Cooper *et al.*, 1989; Cooper, 1990). Cooper and Kohlstedt (1984b) performed hot pressing experiments on crushed olivine-synthetic basalt mixtures under controlled oxygen partial pressures. The densification rate was monitored as a function of applied "hydrostatic" pressure (5-30 MPa) at high temperatures (1300-1400°C) on olivine (basalt) sintered aggregates with final grain sizes of 3-13 μm. With the exception of an enhanced densification rate of a factor of 3 to 5 in the solid-liquid aggregates over the melt-free specimens, both exhibited nearly identical rheologies. Using a grain size dependent form of the semi-empirical flow law for steady-state creep (Eqn. 5.44), Cooper and Kohlstedt (1984a) proposed a stress exponent (n) of unity, an activation enthalpy Q^*_{creep} of 380±125 kJ mol^{-1} and a linear relationship between log $\dot{\varepsilon}$ (strain-rate) and log d (grain size) for olivine aggregates with and without melt. They found microstructural evidence for densification creep enhancement by a solution-precipitation (pressure solution)

mechanism, although the similarity in flow parameters for melt-free olivine and olivine-basalt specimens led them to conclude that diffusive matter transport through melt-free olivine grain boundaries (Cobble creep) was the rate limiting mechanism for densification in olivine-liquid aggregates. This work has been used in determining the bulk viscosity and total effective viscosity (bulk and shear viscosities) for a partially molten peridotite (Richter and McKenzie, 1984; Spiegelman and McKenzie, 1987). As pointed out by Stevenson (1989), however, the compaction process described in these experiments differs from that defining the bulk viscosity of an olivine-melt system, as it occurs through the collapse of a void space, not through the expulsion of liquid. As a consequence, although some authors have estimated an effective viscosity for solid-liquid aggregates (Cooper *et al.*, 1989; Cooper, 1990), there exist no measurements of the bulk viscosity of natural or analog systems applicable to the crust or mantle. From Cooper's (1990) experiments, it appears that the bulk viscosity is of the same order or smaller than the effective shear viscosity and that a pressure-solution mechanism is responsible for both compaction and shear deformation. Although this interpretation is likely to be correct for synthetic aggregates with submicron to micron grain sizes, the applicability to a mantle system with mm to cm grain sizes remains uncertain. Regardless of the deformation mechanism(s), however, this work illustrates the control of the solid matrix on compaction and melt migration.

b. Steady State Deformation at Low Melt Fraction

Experiments on the steady-state shear deformation of rocks in the presence of low melt fractions have been attempted. Avé Lallemant and Carter (1970) observed partial melting in a lherzolite deformed at 1.5 GPa pressure in a solid medium apparatus but did not distinguish or characterize the hypersolidus mechanical behavior. Uniaxial deformation of partially melted dolerite and micro-granodiorite at low confining pressure was studied by Murrell and Chakravarty (1973). However, the specimens were unsealed and early cohesive failure occurred. Several experimental studies on the deformation of partially melted "granitic" rocks have also been undertaken in which brittle fractures were induced by high fluid pressures (Murrell and Ismail, 1976; Van der Molen and Paterson, 1979; Pacquet *et al.*, 1981). Steady state creep experiments at low stresses (0.1-10 MPa) on "dry" partially molten granite under hydrostatic pressure (Auer *et al.*, 1981) indicate that for a melt fraction of up to 20%, the creep behavior was similar to that of a solid (power-law creep) for strains below 10%. Unlike the case for mantle compositions, the melt phase in these systems was not interconnected at low melt fractions (see melt topology section below). These

results are consistent with experiments on a eutectic alloy (Auten *et al.*, 1974; Auten and Gordon, 1975) which show that after transient effects involving melt film redistribution, steady-state flow occurs at a stress level similar to that in the unmelted state. Finally a study of natural and synthetic aplite (Dell'Angelo and Tullis, 1988) which deform by dislocation (power-law) creep in the absence of melt, indicates that the partially molten material properties are dependent on grain size, strain-rate and melt fraction.

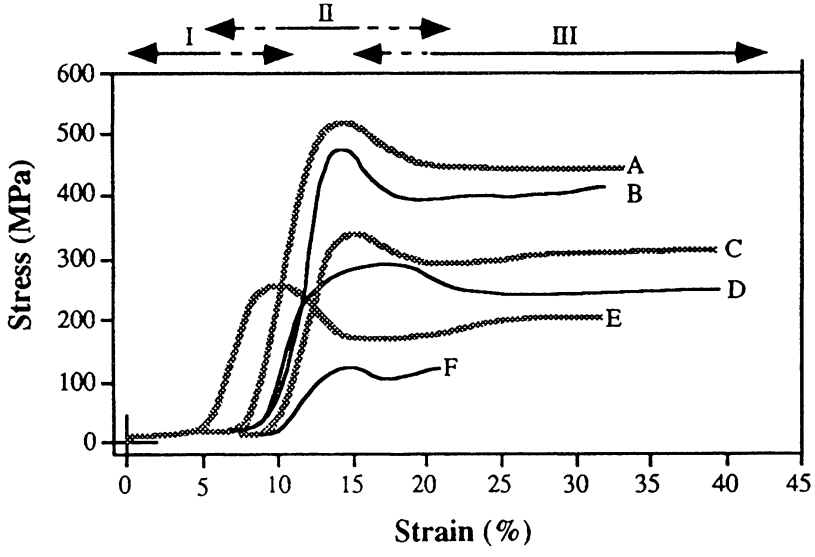

Figure 5.21. Measured stress-strain curves at different strain-rates for partially molten lherzolite at 900°C (heavy gray lines) and 1000°C (thin black lines) or with 1-2% and 5-6% melt respectively. Curves A-B, C-D and E-F are for strain-rates of 10^{-5}, 10^{-6} and 10^{-7} sec^{-1} respectively. The deformation history is separated into 3 regimes (I, II, III) based on mechanical behavior and microstructure (see text).

Deformation experiments on a natural lherzolite at hypersolidus temperatures (Bussod, 1990; Bussod and Christie, 1991) and for melt fractions of 1 to 7 vol.% revealed the rheologic behavior below a critical applied stress of 500 MPa was best described by a nearly temperature insensitive power law (n=3, Q*=200 kJ mol^{-1}; *e.g.* Eqn. 5.44). Whereas the melt is first distributed in melt pools, hypersolidus deformation involves three regimes, in terms of increasing strain (see Fig. 5.21):

I A transient stage associated with melt redistribution (melt squirt) along grain

boundaries and compaction of the solid framework by fracturing (ε=0-10%).

II A pseudo-elastic response of the relatively large grain size (0.5 mm diameter) olivine matrix caused by the interlocking of grains until the yield point at which time cataclastic-plastic behavior leads to the formation of a shear zone at 30° to the maximum principal compressive stress, σ_1 (ε=5-20%).

III Grain size reduction (10-50 μm diameter) via a dislocation creep mechanism (dynamic recrystallization) and the establishment of an interconnected network of melt channels along grain interfaces oriented 30° to σ_1 ($20\% < \varepsilon \leq 45\%$).

These experiments were done at high confining pressures (~1 GPa) and constant volume, thereby involving high fluid pressures. It is therefore likely that regimes II and III involved frictional mechanisms (the relative movement of grains), and dilatant effects as well as solid-state creep. For melt fractions of 1 to 2 vol.% and 4 to 6 vol.%, the measured effective shear viscosities at laboratory conditions (100 MPa $\leq \sigma \leq$ 450 MPa, $\dot{\varepsilon} = 10^{-7}$ s^{-1}) were reduced by a factor of 4 to 5.5, respectively, as compared to the subsolidus lherzolite, and are of the same order of magnitude as the compaction viscosity of olivine-liquid aggregates (Cooper, 1990).

5.5.3. Melt Segregation

When addressing magma segregation processes one must first distinguish the physico-chemical environment (P-T-composition-time path) involved in the generation and transport of the liquid phase. These constraints will dictate the conditions under which magmas will segregate, and the transport process(es) involved. Both mechanisms of fracture and porous flow are equally viable transport processes. In crustal systems transport by magmafracting is most likely as liquids will tend to be isolated in pockets at triple grain edges allowing large fluid pressures to form. Because this is an advective form of transport this is also the most efficient transport process for a relatively cold crustal environment and chemical exchange during transport will be limited.

Magma transport by fracture processes at any depth in the Earth, generally involves the embrittlement of rocks by excess fluid pressures. Though important, this topic is complex and poorly understood as it relates to transient phenomena comprising the initiation of brittle failure and fracture propagation and will not be covered in this chapter.

Conversely in an asthenospheric mantle one might expect porous flow (percolation) to be a dominant mechanism, provided the surrounding mantle remains above its solidus temperature. This is likened to a diffusive transport mechanism and will correspondingly involve various degrees of chemical

exchange between the liquid and its surroundings. In the lithospheric mantle between the crust and convecting mantle, both percolation and fracture mechanisms are likely.

Magma transport by percolation has been studied in greater detail over the past few years and has been modeled using simple two-phase flow theory involving the plastic deformation of the solid matrix. In a closed porous system, liquid cannot escape unless the solid matrix compacts to fill the space it leaves (McKenzie, 1984; Scott and Stevenson, 1984, 86; Fowler, 1985). It has been argued (Walker *et al.*, 1978; Ahern and Turcotte, 1979; Maaløe and Scheie, 1982) that the rate at which the matrix will compact will be governed only by the rate at which the melt can be expelled, and not by the mechanical properties of the matrix. Using two phase flow theory, however, McKenzie (1984) has demonstrated that melt segregation is proportional to the effective differential pressure gradient between the solid and liquid phases. This pressure gradient includes non-hydrostatic pressure gradients associated with shear deformation (shear viscosity) and compaction (bulk viscosity) of the solid framework, and the differential buoyancy of the melt. The expulsion rate is therefore dependent on the viscosity of the solid matrix.

These predictions, however, are based on a simple one dimensional two-phase flow model in which solid and liquid do not react (no *in-situ* melting) and for which, mass and momentum are conserved. In the more general case, the rate-limiting mechanism for melt segregation will depend on the boundary conditions, and whether it is an open or closed system (Ribe, 1987). Whereas in a closed system, theory predicts that the kinetics of melt migration will be rate-limited by the slower of two processes involving liquid flow and plastic deformation of the matrix, in an open system a liquid may flow freely through a solid matrix, driven by buoyancy, without compaction of the solid framework. The behavior of closed or open systems, however, will greatly depend on the topology of the liquid phase, and as a consequence this topic has been strongly emphasized during the past decade.

a. Melt Topology of Crystal-Liquid Aggregates

In addition to the permeability, the topology of the melt phase will control the electrical conductivity (Shankland and Waff, 1977; Tyburczy and Waff, 1986; Waff, 1974), and the seismic wave velocities and attenuation (Solomon, 1972; O'Connell and Budiansky, 1978; Mavko, 1980; Shankland *et al.* 1981) of a partially molten zone in the Earth's mantle. The assumption that porous flow is a viable process for melt segregation in the mantle is principally dependent on the permeability of rocks at depth, *e.g.* the interconnectivity of the melt phase. It

is well established that surface tension on interfaces between crystalline phases and between crystalline and liquid phases constitute (along with chemical activity gradients) driving forces which allow grain surfaces to reach mechanical and thermodynamic equilibrium in relatively short timescales (200 h), (Waff and Bulau, 1979; Jurewicz and Watson, 1985). The condition for textural equilibrium under hydrostatic stress in a two-phase, partially molten, isotropic system, is one in which the surface forces balance at dihedral edges where two solids and a liquid meet, and the chemical potentials at the interfaces are at equilibrium. This condition is generally expressed in terms of solid and fluid surface energy ratios (Eqn. 5.45) and described geometrically by a constant wetting angle or dihedral angle θ (Smith, 1964; Beere, 1975; Kingery *et al.*, 1976; Bulau *et al.*, 1979) (see Fig. 5.22):

$$\theta = 2 \arccos\left(\frac{\gamma_{ss}}{2\gamma_{sf}}\right) \tag{5.45}$$

where γ_{sf} is the surface tension of the solid-fluid interface, and γ_{ss} is the grain boundary energy. The dihedral angle θ (Fig. 5.22) has been proposed as a morphological stability criterion for fluids in edge and corner regions, in a system containing one or several solid phases (Bulau *et al.*, 1979; Toramaru and Fujii, 1986; Fujii *et al.*, 1986). The fluid is morphologically stable (interconnected) when the dihedral angle is less than 60 degrees. Under most circumstances C-O-H fluids will tend to form isolated pores (θ>60°) such that in the absence of fluid overpressures, such fluids are believed to be immobile (Watson *et al.*, 1990). Conversely, at pressures exceeding 2-3 GPa, non-silicate metasomatic fluids such as carbonate melts, will form a continuously interconnected phase along triple grain edges (Watson *et al.* 1990). For silicate-rich fluids effective wetting angles vary with melt composition and mineralogy (Jurewicz and Watson, 1985; Waff and Bulau, 1982; Toramaru and Fujii, 1986; Fujii *et al.*, 1986), but generally fall in the range 10° to 45° for olivine in contact with a wide range of basaltic liquid compositions (Watson *et al.*, 1990). Hydrostatic experiments at 1 GPa pressure, 1300°C on a spinel lherzolite demonstrate, however, that the connectivity of the melt phase is imperfect due to the presence of pyroxene (Toramaru and Fujii, 1986). "Dry" basaltic melts in peridotites are expected to be interconnected only for olivine modal proportions which exceed 80% (dunite or harzburgite). Volatile-rich basaltic melt systems, however, may be permeable for all melt fractions in peridotites (Fujii *et al.*, 1986; Watson *et al.*, 1990), regardless of their modal pyroxene content. These studies all indicate that for hydrostatic conditions, an upper mantle fluid should

never form a grain boundary film. These results seem inconsistent wi observations of mantle xenoliths where grain boundary films are pervasi (Drury and van Roermund, 1989), and experimental evidence on the effect non-hydrostatic stress on melt geometry (Bussod and Christie, 1991). Mo recently, Waff and Faul (1992) have demonstrated that in long duratic "hydrostatic" piston cylinder experiments grain boundary films were common f melt percentages down to 1 vol.% and they attributed this to an equilibriu texture for anisotropic aggregates (Fig. 5.23a,c). If this is correct, both crust and mantle environments should involve the anisotropic distribution of the me phase.

b. Melt Topology in a non-Hydrostatic Stress Regime

Early observations on the distribution of melt in experimentally deforme lherzolites led Avé Lallemant and Carter (1970) to erroneously conclude that lo melt fractions would not segregate from the mantle. Cooper and Kohlstec (1984a) similarly used their results on densification of olivine melt aggregates t conclude that deviatoric stresses had no effect on melt topologies. In the steady state deformation experiments on natural lherzolite at hypersolidus condition Bussod and Christie (1991) described the melt topology as anisotropicall redistributed as melt slots within a network of recrystallized neoblasts (see Fig 5.23b,d). Before the study of Waff and Faul (1992), hydrostatic experiments o basaltic systems seemed to indicate that the melt phase was restricted to tripl grain edges forming interconnected tubular channels. The unique melt topolog from the deformed specimens of Bussod and Christie (1991) was therefor interpreted as resulting from non-hydrostatic stresses and the development of strong olivine lattice preferred orientation by dynamic recrystallization. Th recent hydrostatic experiments of Waff and Faul (1992) appear to indicate tha basaltic melts preferentially "wet" (010) faces of olivine, whereas th deformation experiments of Bussod and Christie (1991) indicate that the lo surface energy (010) faces are generally devoid of melt. This can be reconciled i terms of the strong preferred crystallographic orientation developed in th deformed samples in which the [010] olivine axes are preferentially aligned sub parallel to the maximum principal compressive stress. This is consistent wit the melt being forced out of boundaries with maximum normal stress (normal t the compression axis), such as (010), and consequently restricted to th remaining low energy {hk0} and F-faces (Bussod and Christie, 1991). Th anisotropic orientation of the melt slots along grain interfaces is also distinguishing feature of the deformed specimens and may be due to combine frictional effects (dilatancy) and texture (anisotropy).

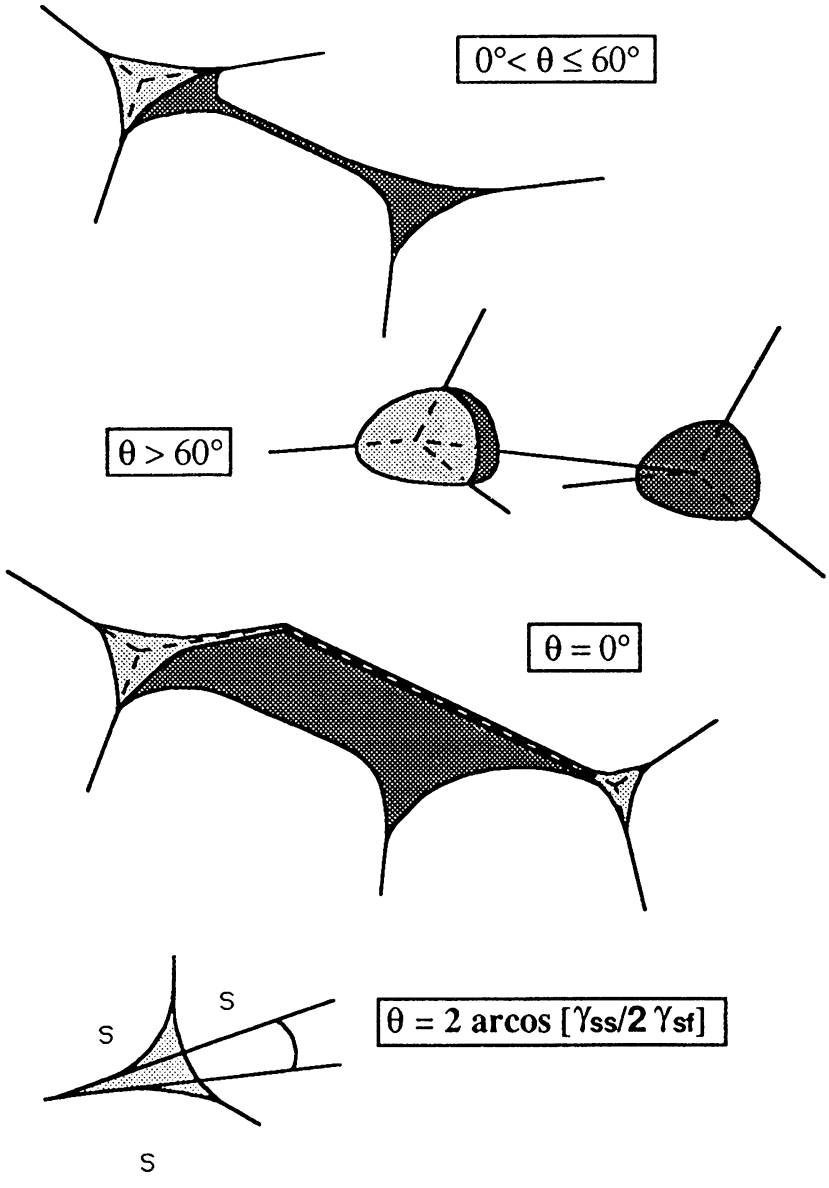

Figure 5.22. Idealized representation of melt topologies based on dihedral angle θ.

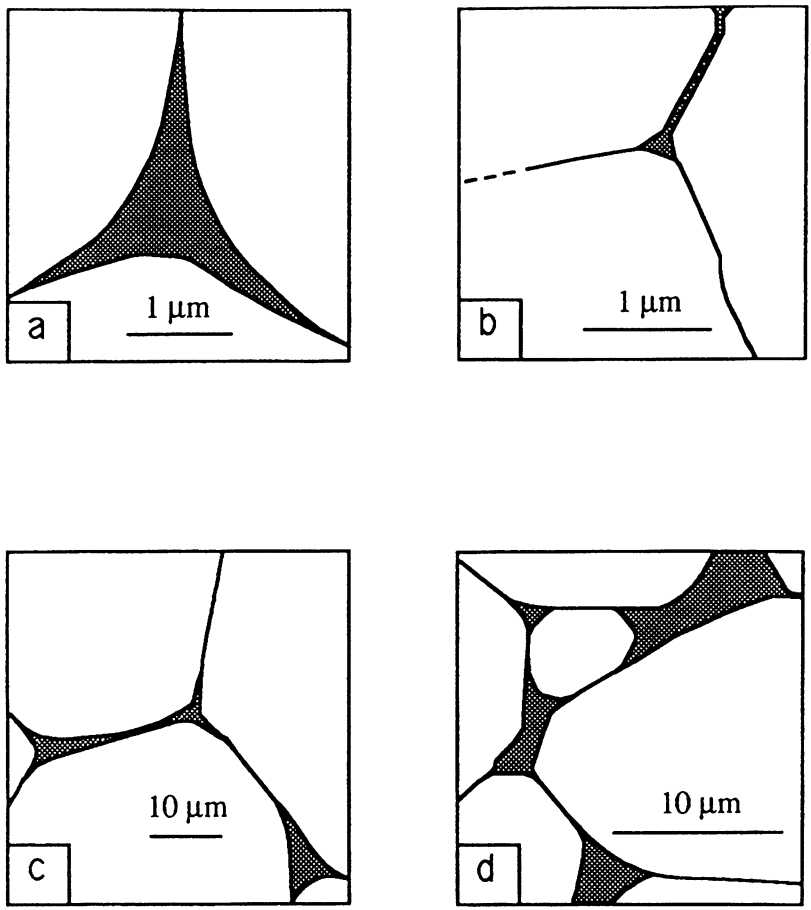

Figure 5.23. Tracings of melt distribution for olivine basalt systems (a,c) under hydrostatic (Waff and Faul, 1992) and (b,d) non-hydrostatic conditions (Bussod, 1990; Bussod and Christie, 1991) for approximately 1 vol.% (a,b) and 5 vol.% (c,d) melt fraction. Stippled area represents quenched melt. BSE image tracings of three grain edge intersections with (a) nearly constant mean curvature and (b) flat interfaces for samples with less than 1% melt. (b) Tracing of TEM photomicrograph representing a triple grain junction between recrystallized olivine neoblasts in a sample with 1 vol.% melt, deformed for 359 hours at T=900°C, P=1 GPa, $\dot{\varepsilon}=1.6\times10^{-7}s^{-1}$, $\sigma_1=195$ MPa. (d) BSE tracing of sample at temperature 119 hours in the presence of 5 vol.% melt and deformed at T=1000°C, P= 1 GPa, $\dot{\varepsilon} = 2.1\times10^{-6}\ s^{-1}$, $\sigma_1=246$ MPa. In both (b) and (d), the maximum principal compressive stress σ_1 is oriented vertically.

Von Bargen and Waff (1986), have pointed out that the relative importance of a deviatoric stress with respect to the solid-liquid interfacial curvature and energy, is related to the their contributions to the balance of chemical potentials on the solid-liquid interface, and to the interfacial curvature. Assuming a homogeneous mean stress field in the solid, the chemical potential on the solid-liquid interface will be a function of orientation. The contribution of a stress potential to the surface energy, is of the same magnitude as the surface energy-curvature term for stresses of 0.01 to 0.04 MPa (Von Bargen and Waff, 1986). This suggests that a 3-D anisotropic melt geometry similar to that observed in the experimentally deformed specimens, may be possible in the mantle where flow stresses are in the range of 0.1 to 10 MPa (Turcotte and Schubert, 1982; Bussod and Christie, 1987), provided the system is undrained. Under these conditions, these observations suggest that the melt topology observed in the deformed specimens, represents a state of dynamic equilibrium. If both hydrostatic and deformation topologies are correct, then the interconnectivity of the melt phase in an olivine rich mantle with a strong lattice preferred orientation (LPO) is expected to be anisotropic. The exact topology of the melt phase (which faces are wet by melt) is expected to be a function of the fluid pressure, melt fraction and applied stress. Below 1 vol.% melt the liquid may be dominantly restricted to triple grain edges (Waff and Faul, 1992).

5.6. CONCLUSION

The last five years have witnessed a significant improvement in the quality and quantity of rheological data for silicate melts and magmas. A number of new concepts have been introduced and new methods developed.

Silicate melts are now viewed as molecular liquids whose fundamental relaxation involves the self-diffusion of silicon in the liquid. Silicate liquids, at high temperature and long timescales are simple Newtonian liquids.

The mechanistic basis of viscous flow is still unclear in detail. The link of viscosity to the configurational entropy of the silicate liquid appears to be qualitatively and quantitatively successful.

The concept of relaxation timescales in melts has clarified several aspects of melt kinetics. The onset of non-Newtonian viscosity can be broadly predicted using linear viscoelastic theory. Experiments demonstrate that the onset of non-Newtonian viscosity can be effectively normalized using the Maxwell relaxation time of the liquid.

Linear viscoelasticity of melts has been extensively investigated using

ultrasonic and torsional methods. The general form of the relaxation mode centered at the glass transition is now known.

The amount of high pressure viscosity data is still insufficient. The composition-dependence of the pressure derivative of melt viscosity is complex and needs clarification through further experiments.

Models for the composition-dependence of viscosity require revision. The pressure-dependence of viscosity and the non-Arrhenian nature of viscosity are not included in present models.

The proper appreciation of experimental and natural timescales in rheology has clarified the experimental approach to the rheology of multiphase magmas. The deformation of bubbles in the flow of vesicular magma has been investigated experimentally. The deformation of bubbles contributes a significant volume viscosity to the macroscopic flow of vesicular materials.

In crystal-liquid systems at high pressure where the melt fraction is low, the flow behavior is dominated by the deformation of the solid matrix. The exact deformation mechanisms are still poorly constrained as in addition to the usual thermodynamic parameters, they are rate-dependent any vary with texture, melt topology, fluid pressure and applied stress.

At experimental conditions, the initiation of melting in granitic and peridotitic assemblages results in a factor of 2-3 decrease in volume viscosity for melts fractions below 10±2 vol.% whereas this viscosity is reduced by 4-8 orders of magnitude for melt fractions between 10 and 30 vol.% (RCMP). The resulting mechanical instability indicates that in the absence of excess fluid pressures (fracturing), magma segregation may occur by channeling for liquid fractions exceeding 10 vol.%.

Recent studies have redefined the criteria for equilibrium melt topologies. Textural equilibrium as defined by the dihedral angle criteria is restricted to monomineralic, isotropic, equidimensional crystal aggregates. New experimental results at hydrostatic and non-hydrostatic conditions have demonstrated that in mantle and crustal assemblages, for melt fractions of 1 to 10 vol.% the liquid is not necessarily restricted to triple grain edges but "wets" grain boundaries due to the anisotropic properties of the solid phases. This implies that melt segregation by percolation is probably more efficient than previously believed and that the melt distribution and therefore physical properties in partially molten regions of the crust and upper mantle are probably anisotropic.

5.7. REFERENCES

Ahern, J.L. and Turcotte, D.L. (1979) Magma migration beneath an ocean ridge. Earth Planet. Sci. Lett., 45, 115-122.

Allison, E.B., Brock, P. and White, J. (1959) The rheology of aggregates containing a liquid phase. Trans. Br. Ceram. Soc., 58, 495-531.

Angell, C.A. (1984) Strong and fragile liquids. In: Ngai K.L. and Wright, G.B. Relaxations in Complex Systems. Naval Research Lab., Arlington, 345pp.

Arndt, N.T. (1977) Ultrabasic magma and high-degree melting of the mantle. Contrib. Mineral. Petrol., 64, 205-221.

Arzi, A.A. (1978) Critical phenomena in the rheology of partially melted rocks. Tectonophys., 44, 173-184.

Auer, F., Beckhemer, H. and Oehlschlegel, G. (1981) Steady state creep of fine grain granite at partial melting. J. Geophys., 49, 89-92.

Auten, T.A., Gordon, R.B. and Stocker, R. (1974) Q and mantle creep. Nature, 250, 317-318.

Auten, T.A. and Gordon, R.B. (1975) Compressive creep rates of partially melted Al-Ga alloys. Metal. Trans., 6A, 584-586.

Avé Lallemant, H. and Carter, N. (1970) Syntectonic recrystallization of olivine and modes of flow in the upper mantle. Geol. Soc. Am. Bull., 81, 2203-2220.

Avery, J.H. and Ingram, A.W. (1971) Modern Laboratory Physics. Heinemann, London.

Bagdassarov, N.S. and Dingwell, D.B. (1992) Rheological investigation of vesicular rhyolite. J. Volc. Geotherm. Res., 50, 307-322.

Bagdassarov, N.S. and Dingwell, D.B. (1993a) Frequency dependent rheology of vesicular rhyolite. J. Geophys. Res., (in press)

Bagdassarov, N.S. and Dingwell, D.B. (1993b) Experimental deformation of vesicular rhyolite under internal and external stresses. Bull. Volc., 55, 147-154.

Bai, Q., Mackwell, S.J. and Kohlstedt, D. (1991) High temperature creep of San Carlos olivine: 1. Steady state flow laws. J. Geophys. Res., 96, 2441-2463.

Barnes, H.A., Hutton, J.F. and Walters, K. (1989) An Introduction to Rheology. Elsevier, 199pp.

Beere, W. (1975) A unifying theory of the stability of penetrating phases and sintering pores. Acta Metall., 23, 131-138.

Bentley, B.Y. and Leal, L.G. (1986) An experimental investigation of drop deformation and breakup in steady, two-dimensional linear flows. J. Fluid Mech., 167, 241-283.

Bottinga, Y. and Weill D.F. (1972) The viscosity of magmatic silicate liquids: a model for calculation. Am. J. Sci., 277, 438-475.

Brearley, M. and Montana, A. (1989) The effect of CO_2 on the viscosities of silicate liquids at high pressures. Geochim. Cosmochim. Acta, 53, 2609-2616.

Brearley, M., Dickinson, J.E. Jr. and Scarfe, C.M. (1986) Pressure dependence of melt viscosities on the join diopside-albite. Geochim. Cosmochim. Acta, 50, 2563-2570.

Brückner, R. and Demharter, G. (1975) Systematische Untersuchung über die Anwendbarkeit von Penetrationsviskosimetern. Glastchn. Ber., 48, 12-18.

Buckmaster J.D., (1972) Pointed bubbles in slow viscous flow. J. Fluid Mech., 55, 385-400.

Bulau, J.R., Waff, H.S. and Tyburczy, J.A. (1979) Mechanical and thermodynamical constraints on fluid distribution in partial melts. J. Geophys. Res., 84, 6102-6108.

Burnham C.W. (1963) Viscosity of a water rich pegmatite. Spec. Pap. Geol. Soc. Am., 76, 26.

Bussod, G.Y. (1990) The experimental deformation of spinel lherzolite at subsolidus and hypersolidus conditions. PhD. Thesis, Univ. California, Los Angeles, 186pp.

Bussod, G.Y. and Christie, J.M. (1987) Deformation mechanisms in experimentally deformed lherzolite at hypersolidus conditions. EOS, 68, 423.

Bussod, G.Y. and Christie, J.M. (1991) Textural development and melt topology in spinel lherzolite experimentally deformed at hypersolidus conditions. J. Petrol., Special Volume, "Orogenic Lherzolites and Mantle Processes", 17-39.

Bussod, G.Y, Katsura, T. and Rubie, D.C. (1992) A new method to experimentally determine the rheologic properties of transition zone minerals at high P-T. EOS, Trans. Am. Geophys. Union, 73, 556.

Chong, J.S., Christiansen, E.B. and Baer, A.D. (1971) Rheology of concentrated suspensions. J. Appl. Polymer. Sci., 15, 2007-2021.

Cooper, R.F. (1990) Differential stress-induced melt migration: An experimental approach. J. Geophys. Res., 95, 6979-6992.

Cooper, R.F. and Kohlstedt, D.L. (1984a) Solution-precipitation enhanced diffusional creep of partially molten olivine-basalt aggregates during hot-pressing. Tectonophys., 107, 207-233.

Cooper, R.F. and Kohlstedt, D.L. (1984b) Sintering of olivine and olivine-basalt aggregates. Phys. Chem. Mineral., 11, 5-16.

Cooper, R.F. and Kohlstedt, D.L. (1986) Rheology and structure of olivine-basalt partial melts. J. Geophys. Res., 91, 9315-9323.,

Cooper, R.F., Kohlstedt, D.L. and Chyung, K. (1989) Solution-precipitation enhanced creep in solid-liquid aggregates which display a non-zero dihedral angle. Acta Metall., 37, 1759-71.

Dabak, T. and Yucel, O. (1986) Shear viscosity behavior of highly concentrated suspensions at low and high shear-rates. Reologica Acta, 25, 527-533.

Dane, E.B. and Birch, F. (1938) The effect of pressure on the viscosity of boric anhydride glass. J. Appl. Phys., 9, 669-674.

Danek, V., Licko, T., Uhrik, M. and Silney, A. (1983) High temperature oscillation viscometer. Silikaty, 27, 333-341.

Danek, V., Licko, T. and Panek, Z. (1985) Viscosity of melts in the system CaO-FeO-Fe_2O_3-SiO_2 Silikaty, 29, 291-299.

Dell'Angelo, L.N. and Tullis, J. (1988) Experimental deformation of partially melted granitic aggregates. J. Metamorph. Geol., 6, 495-515.

Dingwell, D.B. (1987) Melt viscosities in the system $NaAlSi_3O_8$-H_2O-F_2O_{-1}. Geochemical Society Special Publication, 1, 423-433.

Dingwell, D.B. and Mysen, B.O. (1985) Effects of water and fluorine on the viscosity of albite melt at high pressures. Earth Planet. Sci. Lett., 74, 266-274.

Dingwell, D.B. and Webb, S.L. (1989) Structural relaxation in silicate melts and non-Newtonian melt rheology in geological processes. Phys. Chem. Mineral., 16, 508-516.

Dingwell, D.B., Knoche, R., Webb, S.L. and Pichavant, M. (1992) The effect of B_2O_3 on the viscosity of haplogranitic liquids. Am. Mineral., 77, 467-471.

Dunn, T. and Scarfe, C.M. (1986) Variation in the chemical diffusivity of oxygen and viscosity of an andesite melt with pressure at constant temperature. Chem. Geol., 54, 203-216.

Drury, M.R. and Van Roermund, H.L.M. (1989) Fluid assisted recrystallization in uppermost peridotite xenoliths from kimberlites. J. Petrol., 30, 133-152.

Einstein, A. (1911) Eine neue Bestimmung der Moleküldimensionen. Ann. Phys., 19, 289-306.

Evenson, G.F., Ward, S.G. and Whitmore, R.L. (1951) Theory of size distribution; paints, coals, greases, etc. Anomalous viscosity in model suspensions. Farad. Soc. Disc., 11, 11-14.

Ferry, J.D. (1980) Viscoelastic Properties of Polymers. Wiley, New York, 641pp.

Fontana, E.H. (1970) A versatile parallel-plate viscosimeter for glass viscosity measurements to 1000°C. Am. Ceram. Soc. Bull., 49, 594-597.

Fowler, A.C. (1985) A mathematical model for magma transport in the asthenosphere. Geophys. Astrophys. Fluid Dyn., 33, 63-96.

Frankel, N.A. and Acrivos, A. (1970) The constitutive equation for emulsions. J. Fluid Mech., 44, 65-78.

Frost, T.P. and Lindsay, J.R. (1988) MAGMIX: a BASIC program to calculate viscosities of interacting magmas of differing composition, temperature, and

water content. Comp. Geo., 14, 213-228.

Fujii, T. and Kushiro, I. (1977) Density, viscosity and compressibility of basaltic liquid at high pressures. Carnegie Inst. Year Book, 76, 419-424.

Fujii, N., Osamura, K. and Takahashi, E. (1986) Effect of water saturation on the distribution of partial melt in the olivine-pyroxene-plagioclase system, J. Geophys. Res., 91, 9253-9259.

Fulcher, G.S. (1925a) Analysis of recent measurements of the viscosity of glass. I. J. Am. Ceram. Soc., 12, 339-355.

Fulcher, G.S. (1925b) Analysis of recent measurements of the viscosity of glass. II. J. Am. Ceram. Soc., 12, 789-794.

Gay, E.C., Nelson, P.A. and Armstrong, W.P. (1969) Flow properties of suspensions with high solids concentration. AIChE Journal, 15, 815-822.

Gent, A.N. (1960) Theory of the parallel plate viscosimeter. Brit. J. Appl. Phys., 11, 85-88.

Green, H.W. II and Borsch R.S. (1990) High pressure and temperature deformation experiments in a liquid confining medium. In: The Heard Volume. A.G. Duba *et al.* (Eds.), AGU, Washington, 195-200.

Hazen, R.M. and Sharpe, M.R. (1983) Radiographic determination of the positions of platinum spheres in density-viscosity studies of silicate melts. Carnegie Inst. Wash. Yearb., 82, 428-430.

Herzfeld, K.F. and Litovitz, T.A. (1959) Absorption and Dispersion of Ultrasonic Waves. Academic Press, 535pp.

Hessenkemper, H. and Brückner, R. (1989) Load-dependent relaxation behavior of various glassmelts with different structural configurations. Glastech. Ber., 63, 1-6.

Hummel, W. and Arndt, J. (1985) Variation of viscosity with temperature and composition in the plagioclase system. Contrib. Mineral Petrol., 90, 83-92.

Jurewicz, S.R. and Watson, E.B. (1985) The distribution of partial melt in a granitic system. The application of liquid phase sintering theory. Geochim. Cosmochim. Acta, 49, 1109-1121.

Kanzaki, M., Kurita, K., Fujii, T., Kato, T., Shimomura, O. and Akimoto, S. (1987) A new technique to measure the viscosity and density of silicate melts at high pressure. In: High-Pressure Research in Mineral Physics, Manghnani, M.H. and Syono, S. (Eds.), AGU, Washington, 195-200.

Katahara, K.W., Rai, C.S., Manghnani, M.H., and Balogh, J. (1981) An interferometric technique for measuring velocity and attenuation in molten rocks. J. Geophys. Res., 86, 11779-11786.

Kingery, W.D., Bowen, H.K. and Uhlmann, D.R. (1976) Introduction to Ceramics. Wiley-Interscience, New York, 1032pp.

Koch, P.S. (1983) Rheology and microstructures of experimentally deformed quartz aggregates. Ph.D. Thesis, Univ. California, Los Angeles, 464pp.

Kohlstedt, D.L. and Chopra, P.N. (1987) Measurement of rock deformation at high temperatures. Methods of Experimental Physics, 24A, 57-87.

Kraynik, A.M. (1988) Foam flows. Ann. Rev. Fluid Mech., 20, 325-357.

Kushiro, I. (1976) Changes in viscosity and structure of melt of $NaAlSi_2O_6$ composition at high pressures. J. Geophy. Res., 81, 6347-6350.

Lebedev, E.B. and Khitarov, N.I. (1979) Physical properties of magmatic melts. "Nauka" Publ. Moscow, 200pp. (in Russian).

Licko, T. and Danek, V. (1986) Viscosity and structure of melts in the system $CaO\text{-}MgO\text{-}SiO_2$. Phys. Chem. Glass., 27, 22-26.

Maaløe, S. and Scheie, A. (1982) The permeability controlled accumulation of primary magma. Contrib. Mineral. Petrol., 81, 350-357.

Macedo, P.B., Simmons, J.H. and Haller, W. (1968) Spectrum of relaxation times and fluctuation theory: ultrasonic studies on alkali-borosilicate melt. Phys. Chem. Glass., 9, 156-164.

Manghnani, M.H., Rai, C.S., Katahara, K.W. and Olhoeft, G.R. (1981) Ultrasonic velocity and attenuation in basalt melt. In: Anelasticity in the Earth, Geodynamics Series, Volume 4, AGU, 118-122.,

Marsh, B.D. (1981) On the crystallinity, probability of occurrence, and rheology of lava and magma. Contrib. Miner. Petrol., 78, 85-98.

Marshall, L. and Zukovski, C. (1990) Experimental studies on the rheology of hard-sphere suspensions near the glass transition. J. Phys. Chem., 94, 1164-1171.

Mavko, G.M. (1980) Velocity and attenuation in partially molten rocks. J. Geophys. Res., 85, 5173-5189.

Maxwell, J.C. (1867) On the dynamical theory of gases. Phil. Trans. Roy. Soc. London, Ser. A, 157, 49-88.

Mazurin, O.V. (1986) Glass relaxation. J. Non-Cryst. Sol., 87, 392-407.

McBirney, A.R. and Murase, T. (1984) Rheological properties of magmas. Ann. Rev. Earth Sci., 12, 337-357.

McKenzie, J.K. (1950) Elastic constants of a solid containing spherical holes. Proc. Phys. Soc. London, 63, 2-11.

McKenzie, D.P. (1984) The generation and compaction of partially molten rock. J. Petrol., 25, 713-765.

Metzner, A.B. (1985) Rheology of suspensions in polymeric liquids. J. Rheol., 26, 739-775.

Mills, J.J. and Pincus, A.G. (1970) A high shear-rate high temperature rheometer for molten glass. Phys. Chem. Glass., 11, 99-105.

Murase, T., McBirney, A.R. and Melson, W.G. (1985) The viscosity of the dome of Mt. St. Helens. J. Volc. Geotherm. Res., 24, 193-204.

Murrell, S.A.F. and Chakravarty, S. (1973) Some new rheological experiments on igneous rocks at temperatures up to 1120°C. Geophys. J. Roy. Astron. Soc., 34, 211-250.

Murrell, S.A.F. and Ismail, I.A.H. (1976) The effect of temperature on the strength at high confining pressure of granodiorite containing free and chemically-bound water. Contrib. Mineral. Petrol., 55, 317-330.

Nowick, A.S. and Berry, B.S. (1972) Anelastic Relaxation in Crystalline Solids. Academic Press, New York.

O'Connell, R.J. and Budiansky, B. (1978) Measures of dissipation in viscoelastic media. Geophys. Res. Lett., 5, 5-8.

Pacquet, J., Francois, P. and Nedelec, A. (1981) Effect of partial melting on rock deformation: experimental and natural evidences on rocks of granitic compositions. Tectonophys., 78, 545-565.

Panov, V.K., Slezin Y.B. and Stortcheus, A.V. (1985) Mechanical properties of lateral lava flow 'Predskazanniy (1983, volcano Klutchevskaya). Volcanology and Seismology, 1, 21-28. (in Russian).

Persikov, E.S., Zharikov, V.A., Bukhitiyarov, P.G. and Pol'skoy, S.F. (1990) The effect of volatiles on the properties of magmatic melts. Europ. J. Mineral. 2, 621-642.

Pinkerton, H. and Sparks, R.S.J. (1978) Field measurements of the rheology of lava. Nature, 276, 383-384.

Pinkerton, H. and Stevenson, R.J. (1992) Methods of determining the rheological properties of lavas from their physico-chemical properties. J. Volc. Geotherm. Res., 53,47-66.

Pocklington, H.C. (1940) Rough measurement of high viscosities. Proc. Cambridge Phil. Soc., 36, 507-508.

Prud'homme, R.K. and Bird, R.B. (1978) The dilatational properties of suspensions of gas bubbles in incompressible Newtonian and non-Newtonian fluids. J. Non-Newt. Fluid Mech., 3, 261-279.

Ribe, N.M. (1987) Theory of melt segregation - A review. J. Volcanol. Geotherm. Res., 33, 241-253.

Richet, P. (1984) Viscosity and configurational entropy of silicate melts. Geochim. Cosmochim. Acta, 48, 471-483.

Richter, F.M. and McKenzie, D. (1984) Dynamical models for melt segregation from a deformable matrix. J. Geol., 92, 729-740.

Riebling, E.F. (1963) An improved counterbalanced sphere viscometer for use to 1750°C. Rev. Sci. Instr., 34, 568-572.

Riebling, E.F. (1964) Viscosities in the B_2O_3-SiO_2 system. J. Am. Ceram. Soc., 47, 478-483.

Riebling, E.F. (1966) Structure of sodium aluminosilicate melts containing at least 50 mole% SiO_2 at 1500°C. J. Chem. Phys., 44, 2857-2865.

Rivers, M.L. (1985) Ultrasonic studies of silicate melts. Ph.D. Thesis, University of California, 215pp.

Rivers, M.L. and Carmichael, I.S.E. (1987) Ultrasonic studies of silicate melts. J. Geophys. Res., 92, 9247-9270.

Roscoe, R. (1952) The viscosity of suspensions of rigid spheres. Br. J. Appl. Phys., 3, 267-269.

Ryan, M.P. and Blevins, J.Y.K. (1987) The viscosity of synthetic and natural silicate melts and glasses at high temperatures at 1 bar (10^5 Pa) pressure and at higher pressures. U.S. Geol. Surv. Bull. 17864, 563pp.

Ryerson, F.J., Weed, H.C. and Piwinskii, A.J. (1988) Rheology of subliquidus magmas. 1. Picritic compositions. J. Geophys. Res., 93, 3421-3436.

Sato, H. and Manghnani, M.H. (1985) Ultrasonic measurements of V_p and Q_p: relaxation spectrum of complex modulus of basalt melts. Phys. Earth Planet. Int., 41, 18-33.

Scarfe, C.M., Mysen, B.O. and Virgo, D. (1987) Pressure dependence of the viscosity of silicate melts. In: Magmatic Processes: Physicochemical Principles. Geochem. Soc. Spec. Pub., 1, 59-67.

Scholze, H. (1988) Glass - Natur, Struktur und Eigenschaften. Springer, Berlin, 407pp.

Schowalter, W.R. (1978) Mechanics of non-Newtonian fluids. Pergamon Press. Oxford, 300pp.

Schowalter, W.R., Chaffey, C.E. and Brenner, H. (1968) Rheological behavior of a dilute emulsion. J. Coll. Interfac. Sci., 26, 152-160.

Scott, D.R. and Stevenson, D.J. (1984) Magma solitons. Geophys. Res. Lett., 11, 1161-4.

Scott, D.R. and Stevenson, D.J. (1986) Magma ascent by porous flow. J. Geophys. Res., 91, 9283-9296.

Shankland, T.J. and Waff, H.S. (1977) Partial melting and electrical conductivity anomalies in the upper mantle. J. Geophys. Res., 82, 5409-5417.

Shankland, T.J., O'Connell, R.J. and Waff, H.S. (1981) Geophysical constraints on partial melt in the upper mantle. Rev. Geophys., 19, 394-406.

Sharma, S.K., Virgo, D. and Kushiro, I. (1979) Relationships between density, viscosity and structure of GeO_2 melts at low and high pressure. J. Non-Cryst. Solid., 33, 235-248.

Shaw, H.R. (1963) Obsidian-H_2O viscosities at 1000 and 2000 bars in the

temperature range 700° to 900°C. J. Geophy. Res., 68, 6337-6343.

Shaw, H.R. (1972) Viscosities of magmatic silicate liquids: an empirical method of prediction. Am. J. Sci., 272, 870-889.

Shaw, H.R., Peck, D.L., Wright, T.L. and Okamura, R. (1968) The viscosity of basaltic magma: an analysis of field measurements in Makaopuhi lava lake, Hawaii. Am. J. Sci., 272, 870-893.

Sherman, P. (1968) Emulsion Science. Academic Press, New York, 351pp.

Shimozuru, D. (1978) Dynamics of magma in a volcanic conduit - special emph-asis on viscosity of magma with bubbles. Bull. Volcanol., 414, 333-340.

Shiraishi, Y., Granasy, L., Waseda, Y. and Matsubara, E. (1987) Viscosity of glassy Na_2O-B_2O_3-SiO_2 system. J. Non-Cryst. Solid., 95, 1031-1038.

Sibree, J.O. (1934) The viscosity of froth. Trans. Farad. Soc., 30, 325-331.

Simmons, J.H., Ochoa, R. and Simmons, K.D. (1988) Non-Newtonian viscous flow in soda-lime-silica glass at forming and annealing temperatures. J. Non-Cryst. Solid., 105, 313-322.

Smith, C.S. (1964) Some elementary principals of polycrystalline microstructure. Met. Re., 33, 1-48.

Solomon, S.C. (1972) Seismic wave attenuation and partial melting in the upper mantle of North America. J. Geophys. Res., 77, 1483-1502.

Spera, F.J., Borgia, A. and Strimple, J. (1988) Rheology of melts and magmatic suspensions 1. Design and calibration of concentric cylinder viscometer with application to rhyolitic magma. J. Geophys. Res., 93, 10273-10294.

Spiegelman, M. and McKenzie, D. (1987) Simple 2-D models for melt extraction at mid ocean ridges and island arcs. Earth Planet. Sci. Lett., 87, 137-152.

Spray, J. (1993) Viscosity of some frictionally-generated silicate melts: implications for fault zone rheology at high strain rates. J. Geophys. Res., (in press).

Stein, D.J. and Spera, F.J. (1992) Rheology and microstructure of magmatic emulsions: theory and experiments. J. Volc. Geotherm. Res., 49, 157-174.

Stevenson, D.J. (1989) Spontaneous small-scale melt segregation in partial melts undergoing deformation. Geophys. Res. Lett., 16, 1067-1070.

Stocker, R.L. and Ashby, M.F. (1973) On the rheology of the upper mantle. Res. Geophys. Space Phys., 11, 391-426.

Sura, V.M. and Panda, P.C. (1990) Viscosity of porous glasses. J. Am. Ceram. Soc., 73, 2697-2701.

Sweeny, K.H. and Geckler, R.D. (1954) The rheology of suspensions. J. Appl. Phys., 25, 1135-1144.

Tamann, G. and Hesse, W. (1926) Die Abhängigkeit der Viskosität von der Temperatur bei untergekuhlten Flussigkeiten. Z. anorg. allg. Chem., 156,

245-257.

Tauber, P. and Arndt, J. (1986) Viscosity and temperature relationship of liquid diopside. Phys. Earth Planet. Int., 43, 97-103.

Tauber, P. and Arndt, J. (1987) The relationship between viscosity and temperature in the system anorthite-diopside. Chem. Geol., 62, 71-82.

Tauke, J., Litovitz, T.A. and Macedo, P.B. (1968) Viscous relaxation and non-Arrhenius behavior in B_2O_3. J. Am. Ceram. Soc., 51, 158-163.

Taylor, G.I. (1932) The viscosity of fluid containing small drops of another fluid. Proc. Roy. Soc. London. Ser A, 138, 41-48.

Tobolsky, A.V. and Taylor, R.B. (1963) Viscoelastic properties of a simple organic glass. J. Phys. Chem., 67, 2439-2442.

Toramaru, A. and Fujii, N. (1986) Connectivity of melt phase in a partially molten peridotite. J. Geophys. Res., 86, 9239-9252.

Tørklep, K. and Øye, H.A. (1979) An absolute oscillating cylinder (or cup) viscometer for high temperatures. J. Phys. E.: Sci. Instrum., 12, 875-885.

Turcotte, D.L. and Schubert, G. (1982) Geodynamics: Application of continuum physics to geologic problems. John Wiley, New York.

Tyburczy, J.A. and Waff, H.S. (1986) Electrical conductivity of molten basalt and andesite to 25 kilobars pressure: Geophysical significance and implications for charge transport and melt structure. J. Geophys. Res., 88, 2413-2430.

Utracki, L.A. (1988) The rheology of two-phase flows. In: Rheological Measurements, Collyer, A. and Clegg, D. (Eds) Elsevier, London, 479-594.

Van der Molen, I. and Paterson, M.S. (1979) Experimental deformation of partially molten granite. Contrib. Mineral. Petrol., 70, 299-318.

Vogel, H. (1921) Das Temperaturabhängigkeitsgesetz der Viskosität von Flussigkeiten. Physik Z., 22, 645-646.

Von Bargen, N. and Waff, H.S. (1986) Permeabilities, interfacial areas, and curvatures of partially molten systems: Results of numerical computations of equilibrium microstructures. J. Geophys. Res., 91, 9261-9276.

Waff, H.S. (1974) Theoretical considerations of electrical conductivity in a partially molten mantle and implications for geothermometry. J. Geophys. Res., 79, 4003-4010.

Waff, H.S. and Bulau, J.R. (1979) Equilibrium fluid distribution in an ultramafic partial melt under hydrostatic stress conditions. J. Geophys. Res., 84, 6109-6114.

Waff, H.S. and Bulau, J.R. (1982) Experimental determination of near-equilibrium textures in partially molten silicates at high pressures, In: Akimoto, S. and Manghnani, M.H. (Eds), Advances in Earth and Planetary Sciences, 12, Center for Academic Publications, Tokyo, 229-236.

Waff, H.S. and Faul, U.H. (1992) Effects of crystalline anisotropy on fluid distribution in ultramafic partial melts. J. Geophys. Res., 97, 9003-9014.

Walker, D., Stolper, E.M. and Hays, J.F. (1978) A numerical treatment of melt/solid segregation: Size of eucrite parent body and stability of terrestrial low velocity zone. J. Geophys. Res., 83, 6005-6013.

Ward, S.G. and Whitmore, R.L. (1950a) Studies of the viscosities and sedimentation of suspensions. 1. The viscosity of suspension of spherical particles. Brit. J. Appl. Phys., 1, 286-290.

Ward, S.G. and Whitmore, R.L. (1950b) Studies of the viscosities and sedimentation of suspensions. 2. The viscosity and sedimentation of suspension of rough powders. Brit. J. Appl. Phys., 1, 325-328.

Watson, E.B., Brenan, J.M. and Baker, D.R. (1990) Distribution of fluids in the continental mantle. In: Continental Mantle, Menzies M.A. (Ed), Clarendon Press, Oxford, 111-125.

Webb, S.L. (1991) Shear and volume relaxation in $Na_2Si_2O_5$. Am. Mineral., 76, 451-456.

Webb, S.L. and Dingwell, D.B. (1990a) Non-Newtonian rheology of igneous melts at high stresses and strain-rates: experimental results for rhyolite, andesite, basalt and nephelinite. J. Geophys. Res., 95, 15695-15701.

Webb, S.L. and Dingwell, D.B. (1990b) The onset of non-Newtonian rheology of silicate melts. Phys. Chem. Mineral., 17, 125-132.

White, B. and Montana, A. (1990) The effect of H_2O and CO_2 on the viscosity of sanidine liquid at high pressures. J. Geophy. Res., 95, 15683-15693.

Wilson, L., Sparks, R.S.J. and Walker, G.P.L. (1980) Explosive volcanic eruptions IV. The control of magma properties and conduit geometry on eruption column behavior. Geophys. J. R. Astron. Soc., 63, 117-148.

Zarzycki, J, (1991) Glasses and the Vitreous State. Cambridge University Press, Cambridge, 505pp.

Zhaohui, W. (1982) Settling velocity of particles in a Bingham fluid. Prog. Rep. Inst. Hydrodyn. Hydr. Eng., Tech. Univ. Denmark, 56, 3-11.

5.8 ACKNOWLEDGEMENTS

We wish to thank Bob Luth and the Mineralogical Association of Canada for their organization and support of this Short Course. We thank Don Baker, George Bergantz and Frank Spera for constructive reviews. This work has been supported, in part, by the A. v. Humboldt Foundation (N.B.) and the Deutsche Forschungsgemeinschaft grant (Di 431/2-1).